Chapter 4

Objective 1

Chitosan/hyaluronic acid-based nanoparticles for spatially targeted delivery of cabazitaxel in DMBA-induced breast tumor in rats

4 Cetuximab functionalized chitosan/hyaluronic acid-based nanoparticles loaded with cabazitaxel to improve the anti-tumor efficacy in DMBA-induced breast cancer models in rats

4.1 Introduction

Breast cancer is one of the most frequent malignancies affecting women worldwide. Approximately 13% (or one in every eight) of women in the United States may acquire invasive breast cancer over their lifetime. In 2023, an estimated 297,790 new instances of invasive breast cancer and about 55,720 new cases of DCIS are predicted to be detected in women in the United States [93]. The traditional treatment of breast cancer includes surgery followed chemotherapy and radiation therapy. However, conventional anticancer drugs are associated with systemic toxicity due to non-targeted distribution to all major organs of body. Loading the chemotherapeutics in nanosized carrier is a promising approach for improving the therapeutic outcomes of breast cancer therapy due to their ability to provide precise and effective delivery of chemotherapeutics to the intended region.

Nanoparticles loaded with chemotherapeutics designed using biopolymers have distinct advantages like, biocompatibility, biodegradability, non-immunogenicity, and non-toxicity [94,95]. Biopolymers like chitosan (CS), gelatin, silk fibroins, collagen, albumin, starch, and cellulose has shown immense potential in formulation of nanoparticles [96]. CS is a natural cationic polysaccharide derived from chitin, found in exoskeletons of insects and mollusks, and shell of crustaceans [97]. Due to the amino groups on its structure, endowing it positive charge it can form nanoparticles with oppositely charged polymers via electrostatic interaction [98,99]. Hyaluronic acid (HA) is a natural anionic (negatively charge) polysaccharide with carboxylic group in its structure [100]. HA has high biocompatibility but rapid degradation, low mechanical integrity and high solubility [101].

HA also has the capability to interact with cell surface receptors and facilitate cellular internalization [102]. Thus, HA-mediated ionic gelation of CS for nanoparticles synthesis is a promising approach for preparation of nanoparticles, leveraging the combined properties of both polymers to create a functional and versatile nanoparticle with spatial targeting capability [99,103].

Present work involved development of HA-mediated ionic gelation of CS to form nanoparticles. Cabazitaxel (CBT), a chemotherapeutics from the taxane category with poor affinity to P-glycoprotein and superior anticancer activity to superior to paclitaxel and docetaxel, was employed as a model lipophilic drug for loading in nanoparticles, in the current study [104]. Numerous research has reported the use of CBT against breast cancer but may also exhibit drug distribution to all major organs other than cancer site [105,106]. This results high dose requirement, organ toxicity and substantial therapeutic effect. These challenges can be addressed by loading drug in targeted nanoparticles for site specific delivery [107–110]. Related to this, various reports of CS and HA based nanoparticles for targeted breast cancer therapy has been made that integrates the ionic gelation mediated assembly of hydrophilic polysaccharides like CS and HA to encapsulate a lipophilic drug with an antibody and PEG anchored corona [101,111]. The presence of an EGFR antibody on the surface of the prepared nanoparticles renders the system targeting behavior, ensuring a selective and intracellular delivery of the therapeutic payload. The PEG layer formed on the surface may be attributed to the use of TPGS in the preparation, while the surface functionalization by Cmab to improve the targeting efficiency of the nanoparticles was performed by exploiting the free carboxylic group of TPGS and conjugating the antibody to the free carboxylic acid via. carbodiimide chemistry [112,113]. The TPGS was succinylated firsthand to achieve a terminal carboxylic acid group on TPGS. The conjugation was successfully confirmed by NMR

and Mass spectroscopy. The nanoparticles were characterized for hydrodynamic diameter, surface charge, degree of conjugation, and other solid-state and surface characteristics. The nanoparticles were evaluated for pH-sensitive release, improved cellular uptake, and increased intracellular accumulation of the payload. The studies further assess pharmacokinetic parameters, vivo anti-tumor efficacy, and survivability. The effect of the off-target distribution of CBT releases from the targeted nanoparticles was also determined by observing the weight loss in animals during the treatment regimen.

4.2 Materials and Methods

4.2.1 Materials

Cabazitaxel (CBT) was obtained from MSN Laboratories as a Gift Sample; Sodium Hyaluronate (HA) with an average molecular weight of ~7.6 kDa was provided by Shandong Topscience Biotech Co. Ltd., Shandong, PRC. D-alpha-Tocopheryl polyethylene glycol 1000 succinate (TPGS) was a gift sample from Antares Health Products, St. Charles, USA. Chitosan (CS), Succinic anhydride (SA), N, 4-Dimethylaminopyridine (DMAP), and 1-(3-Dimethylaminopropyl)-3-ethylcarbodiimide hydrochloride (EDC) were procured from SRL Pvt. Ltd was procured from SRL Chemicals. Sodium Tripolyphosphate was procured from Sigma Aldrich. MDA-MB-231 and HEK-293 cell lines were obtained from the National Centre for Cell Science (NCCS) in Pune, India. Genetics Biotech Asia Pvt. Ltd. supplied the necessary laboratory materials, including DMEM (Dulbecco's Modified Eagle Medium) and 12-well cell culture plates. T-25 flasks and 96-well plates were provided by Eppendorf. Gibco was the selected supplier for Penicillin-streptomycin, Trypsin-EDTA, and FBS (Fetal Bovine Serum). High-quality analytical-grade chemicals from a reputable brand were utilized to prepare Phosphate Buffer Saline (PBS). All the other chemicals and solvents used in the experiments were high-purity grades

4.2.2 Synthesis and characterization of succinylated TPGS

The D-alpha-tocopheryl polyethylene glycol 1000 succinate (TPGS) terminal hydroxyl group was conjugated with succinic anhydride (**Figure 4.1 A**) [114]. Briefly, 1.543 g of TPGS was lyophilized to remove any residual moisture. The dry TPGS sample was then dissolved in 20 mL of dry methylene chloride in a 100 mL Schlenk flask. The air from the solution was removed using nitrogen gas. SA (180 mg) and DMAP (30 mg) dissolved in 20 mL of methylene chloride were added to the TPGS solution. The reaction vessel was purged with nitrogen gas for 2 minutes and sealed with a nitrogen balloon. The reaction mixture was kept on stirring for 48 h. After the completion of the reaction, the mixture was precipitated in cold diethyl ether (kept overnight at -80 °C for complete precipitation. The precipitate was dissolved in 20 mL water: ethanol (50:50) and dialyzed against water: ethanol mixture (50:50) for 48 h, followed by MilliQ water for 24 h. The purified TPGS-COOH was lyophilized to obtain a white crystalline solid (Yield: 84.28%). The succinylation of TPGS (TPGS-COOH) was confirmed by ^{1}H and ^{13}C Nuclear magnetic resonance (NMR; Bruker AVH D 500 AVANCE III HD), Mass spectrometry (ESI-MS; Agilent 1100LC-QTOF), and Fourier-transform infrared (FTIR; Shimadzu 8400S). X-ray diffraction (XRD; Rigaku Miniflex 600) and Differential scanning calorimetry (DSC; Shimadzu DSC-60 Plus) analysis were also performed for TPGS and TPGS-COOH. Solid-state characterization was performed with lyophilized samples. TPGS and TPGS-COOH were dissolved in deuterated methanol for NMR spectroscopy.

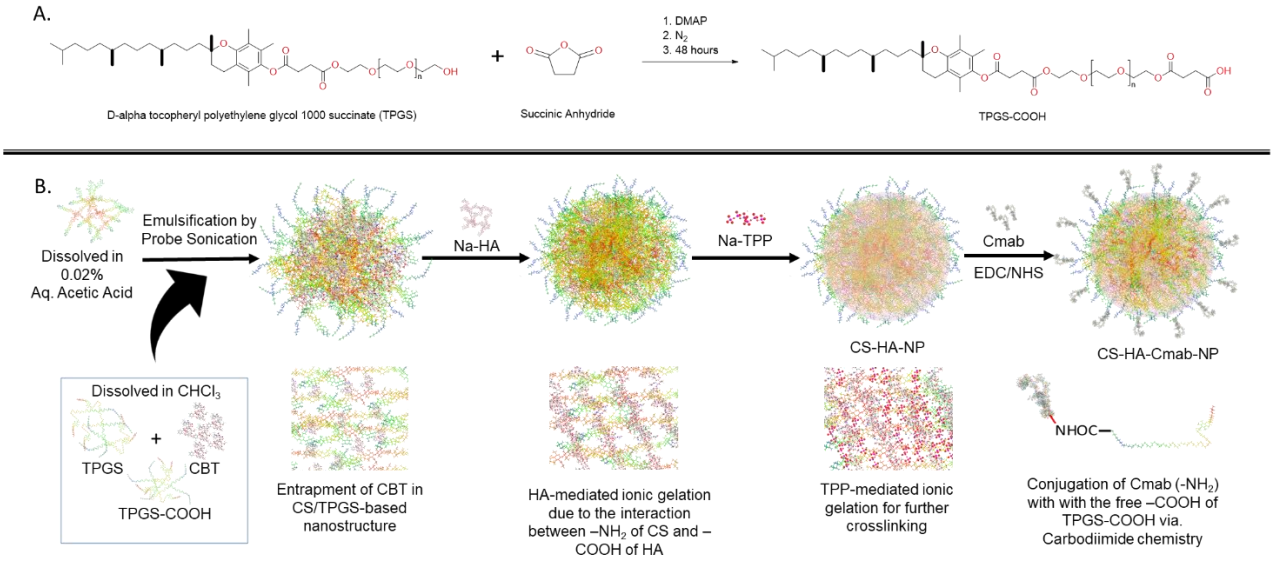

Figure 4.1 (**A**) Conjugation of SA with TPGS. (**B**) Schematic illustration of preparation of CS-HA-NP and CS-HA-Cmab-NP.

4.2.3 Preparation of chitosan/hyaluronic acid-based nanoparticles

The nanoparticles were prepared using a modified ionic gelation method (**Figure 4.1 B**) [115,116]. Firstly, CS (30 mg) and TPGS (20 mg) were dissolved in 6 mL of 0.02 % aqueous acetic acid solution. Cabazitaxel (3 mg) was dissolved in chloroform and added to the CS/TPGS solution. The chloroform and aqueous phase were emulsified using a 1 mm probe sonicator at 60% amplitude for 7 minutes (5 sec ON and 2 sec OFF cycle) on an ice bath. The emulsion was kept on a stirrer at 100 RPM at room temperature for the chloroform to evaporate. Subsequently, 5 mg of HA (1mg/mL solution in double distilled water) was added dropwise to the solution under constant stirring. After stirring the solution for 2 h, 4 mg of sodium tripolyphosphate (1mg/mL solution in double distilled water) was added and stirred for 4 h. The formed nanoparticles (CS-HA-NP) were washed and purified using Amicon® centrifuge filters (MWCO 30 kDa). The nanoparticles were then lyophilized and stored for further analysis. To prepare Cetuximab conjugated nanoparticles (CS-HA-Cmab-NP), CS-HA-NP was prepared as before with 10 mg each of

TPGS and TPGS-COOH taken instead of 20 mg of TPGS. The particles were washed and resuspended in double distilled water, and 19 mg of EDC and 12 mg of NHS were added to activate the carboxylic group of TPGS-COOH. The activation was allowed for 30 minutes, and then Cmab 2 mg was added to the suspension. The reaction mixture was stirred for 2 h to allow cetuximab conjugation on the surface of the nanoparticles.

To prepare coumarin-6 loaded nanoparticles (c6CS-HA-NP and c6CS-HA-Cmab-NP), 0.1 mg of coumarin-6 (C6) was added with CBT in chloroform before the sonication step. Chloroform, without CBT and C6, was used in the emulsification step to prepare blank nanoparticles (bCS-HA-NP). The composition of various batches are listed in **Table 4.1** .

Table 4.1 Composition of CS-HA-NP and CS-HA-Cmab-NP nanoparticles

Batch Code	CS (mg)	TPGS (mg)	TPGS-COOH (mg)	sHA (mg)	sTPP (mg)	CBT (mg)	C6 (mg)	Cmab (mg)
bCS-HA-NP	30	20	--	5	4	--	--	--
CS-HA-NP	30	20	--	5	4	3	--	--
CS-HA-Cmab-NP	30	10	10	5	4	3	--	2
c6CS-HA-NP	30	20	--	5	4	3	0.1	--
c6CS-HA-Cmab-NP	30	10	10	5	4	3	0.1	2

4.2.4 Physicochemical characterization of nanoparticles

4.2.4.1 Hydrodynamic size, Zeta potential, and Particle morphology

The hydrodynamic size and zeta potential of the prepared nanoparticles (CS-HA-NP and CS-HA-Cmab-NP) were determined by photon correlation spectroscopy (PCS) using Malvern Zetasizer (Nano ZS, Malvern Instruments, UK) [117,118]. The morphology was determined using electron microscopy and a scanning probe microscope (SPM). Freshly prepared nanoparticle suspensions were diluted with MilliQ water, and a drop was cast on the glass slides and copper-coated TEM grids [102,113]. The samples were vacuum-dried overnight at room temperature. The copper-coated TEM grids were observed using TEM (Technai G2 20 TWIN; FEI, USA), while the glass slide was gold-coated and observed using SEM (Nova Nano SEM 450; FEI, USA). The glass slide without gold coating was scanned using SPM (NTEGRA Prima, NT-MDT BV, Netherlands) to assess particle surface smoothness and grain distribution. The image analysis was done using Nova Powerscript.

4.2.4.2 Solid state characterization

The solid-state characterization of the drug, polysaccharides, and targeted and non-targeted nanoparticles was done by FT-IR, XRD, DSC, and XPS (X-ray photoelectron spectroscopy) [113,119]. The FTIR spectra of lyophilized neat CBT, CS, HA, CS-HA-NP, and CS-HA-Cmab-NP powder were recorded at a resolution of 2 cm^{-1} between 4000 cm^{-1} to 400 cm^{-1} using a KBr pellet. The XRD study assessed the diffraction pattern of all the samples. The spectra were recorded at a step size of 0.02 degrees and a scan rate of 5 degrees min^{-1} in the 2θ range of 5 to 50 degrees. The DSC was performed in the 0-300 degrees Celsius temperature range with a 20-degree min^{-1} rate. The elemental composition of the surface of nanoparticles was identified using XPS (K-Alpha model with Mg Kα

radiation (hν = 1253.6 eV); Thermo Fisher Scientific) in the range of 100-700 eV binding energy.

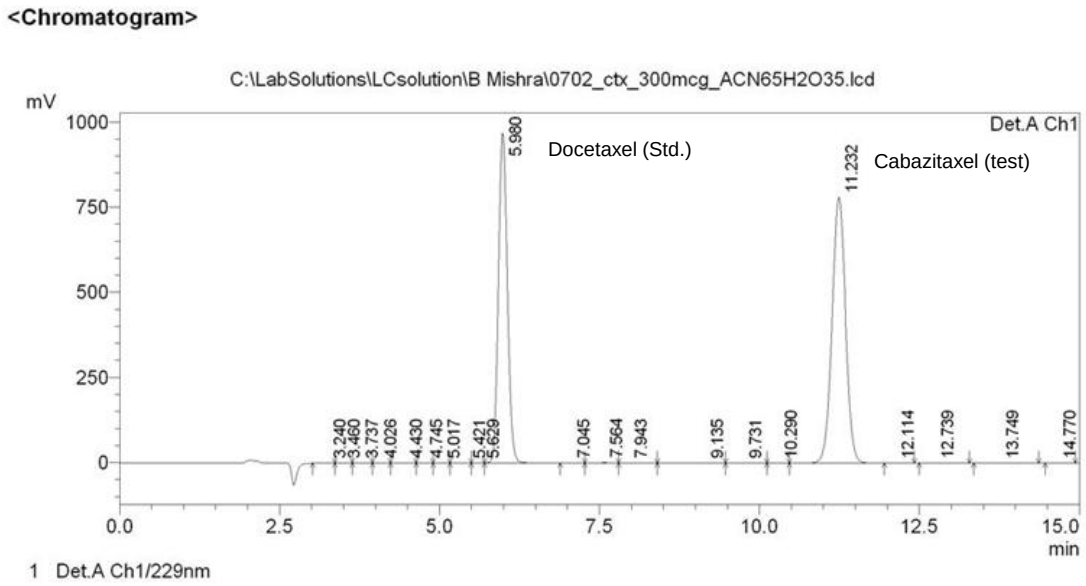

Figure 4.2 HPLC Chromatogram of Cabazitaxel (RT- 5.98 min) and Docetaxel (RT- 11.23)

4.2.5 Analytical method development

An analytical method was developed to quantitatively estimate CBT using high-performance liquid chromatography (HPLC) equipped with a UV detector (HPLC, Shimadzu, Japan). A reverse phase C18 column (150 mm length, 4.6 mm diameter, and 5 µm particle size) and mobile phase composed of Acetonitrile (76 percent) and 0.3% acetic acid in MilliQ water (24 percent) was used to elute the analyte at a flow rate of 1 mL/min. The eluent was observed at the wavelength of 229 nm. **Figure 4.2** shows the HPLC chromatogram of CBT with internal standard DTX at 229 nm.

4.2.6 Encapsulation efficiency, drug loading, and degree of conjugation

To determine the encapsulation efficiency, freshly prepared nanoparticles (CS-HA-NP and CS-HA-Cmab-NP) were dispersed in a 10 mL of water-methanol mixture (1:1 v/v) [113]. The suspension was sonicated at 80% amplitude for 10 minutes on ice bath using a 1 mm

probe. The suspension was then filtered using Amicon® centrifuge filter (MWCO-30kDa). The 20 µL of the filtrate was then injected into the HPLC to determine the CBT concentration using the earlier method. The encapsulation efficiency (EE) was determined using the formula [120];

$$EE\ (\%) = \frac{Amount\ of\ drug\ detected\ in\ nanoparticles\ (mg)}{Amount\ of\ drug\ added\ in\ the\ preparation\ of\ nanoparticles\ (mg)} \times 100$$

A similar method was followed to determine the percentage drug loading (DL), except in place of freshly prepared nanoparticles, 100 mg of lyophilized nanoparticles were taken. Drug loading was calculated using the formula [120];

$$DL\ (\%) = \frac{Amount\ of\ drug\ detected\ in\ nanoparticles\ (mg)}{Weight\ of\ nanoparticles\ taken\ (mg)} \times 100$$

A Bradford assay was performed to determine the degree of conjugation of Cmab on the surface of the nanoparticles [112,121]. Bovine serum albumin (BSA) was used as a standard protein to plot a calibration curve. Predetermined concentrations of BSA were incubated with Bradford's reagent, which gave color change after incubation. The absorbance of BSA bound reagent was observed at 595 nm wavelength, and a concentration versus absorbance graph was plotted. This calibration curve was used to determine the degree of conjugation of Cmab on the surface of nanoparticles. Freshly prepared, washed, and purified CS-HA-Cmab-NPs were incubated with Bradford's reagent for 5 minutes, and the absorbance was noted at 595 nm wavelength. The absorbance was extrapolated against the calibration curve to determine the amount of cetuximab conjugated to the nanoparticles.

4.2.7 Drug release study

The drug release study was performed using the dialysis method. CS-HA-NP and CS-HA-Cmab-NP equivalent to 5 mg of CBT were added in a dialysis bag (Spectra/Por® 7 1000 Da MWCO) containing 5 mL of buffered media. The dialysis bag was then immersed in

45 mL of buffered media and stirred at 100 rpm. The temperature was maintained at 37±0.5 °C, and aliquots of 500 µL were withdrawn from the media at predetermined intervals. After each sampling, the release media was replenished with 500 µL of fresh buffered media. The samples were filtered using membrane disc filters with a pore size of 0.10 µm and a diameter of 13 mm. The filtered samples were then analyzed using HPLC to estimate the cumulative percentage of drug release at various time intervals. The drug release was assessed in Phosphate buffered saline (pH 7.4), phosphate buffer (pH 6.8), and acetate buffer (pH 5.5).

4.2.8 In vitro cell line studies

4.2.8.1 Cell line maintenance

FBS (Fetal Bovine Serum) and penicillin-streptomycin solution-enriched DMEM were used to culture MDA-MB-231 (Breast Cancer cell line) and maintained in a humidified CO_2 incubator at 37 °C under 5% CO_2.

4.2.8.2 In vitro cytotoxicity assay

MTT (3-(4, 5-dimethylthiazolyl-2)-2, 5-diphenyltetrazolium bromide) assay was used to estimate the cytotoxicity of CS-HA-NP and CS-HA-Cmab-NP [122]. 1×10^5 MDA-MB-231 cells were seeded per well in a 96-well plate overnight. Subsequently, the cells were treated with various concentrations of bCS-HA-Cmab-NP, neat CBT, CBT-loaded CS-HA-NP, and CBT-loaded CS-HA-Cmab-NP and incubated for 24 h. After 24 h incubation, the cells were further incubated with 100 µL of (5 mg/mL) MTT reagent dissolved in media for another 2 h. The solution was removed, 100 µL of dimethyl sulfoxide was added to the wells, and the absorbance reading was acquired at 570 nm using a microplate reader. The percentage of viable cells in each well was calculated using the formula;

$$Percentage\ cell\ viability\ (\%) = \frac{Absorbance\ of\ sample\ at\ 570\ nm}{Absorbance\ of\ control\ at\ 570\ nm} \times\ 100$$

4.2.8.3 Cellular uptake study

c6CS-HA-NP and c6CS-HA-Cmab-NP and free C6 were used to determine the cellular uptake of the nanoparticles in MDA-MB-231 cells [123]. In a 12-well culture plate, 50000 MDA-MB- 231 cells were seeded and adhered for 24 h. The cells received treatment equivalent to 0.1 µg/mL of C6 and were incubated for six h. Treatment groups included control (untreated), free C6, c6CS-HA-NP, and c6CS-HA-Cmab-NP. To evaluate whether the CS-HA-Cmab-NP shows EGFR-mediated endocytosis, one well was pretreated with cetuximab for 30 min and then treated with c6CS-HA-Cmab-NP. After incubation, the cells were washed with PBS, counterstained with DAPI (10 µg/mL), and observed under the EVOS FL Cell Imaging System in green and blue channels [124].

4.2.8.4 Assessment of nucleus morphology

The Hoechst33342/PI double staining protocol was used to ascertain the effect of nanoparticle treatment on the nucleus morphology [125]. A 12-well culture plate was seeded with 50000 MDA-MB- 231 cells and incubated for 24 h. After incubation, the cells were treated with neat CBT, CS-HA-NP, and CS-HA-Cmab-NP at IC_{50} of CS-HA-Cmab-NP. One well also received a pretreatment 30 minutes before receiving CS-HA-Cmab-NP to perform the blocking study. The cells were again incubated for 24 h. Subsequently, the cells were exposed to PI and Hoechst33342 for 30 minutes at 37°C and washed with PBS. The washed cells were imaged by the EVOS FL Cell Imaging System in the red and blue channels.

4.2.8.5 Assessment of mitochondrial depolarization

To assess the extent of mitochondrial depolarization, a 12-well cell culture plate was seeded with 50000 viable MDA-MB-231 cells in each well and incubated for 24 h. The cells were then treated with neat CBT, CS-HA-NP, and CS-HA-Cmab-NP at

concentrations equal to IC_{50} of CS-HA-Cmab-NP and incubated further for 24 h. After the incubation with various treatments, the cells were incubated with JC-1 (1 μM) for 30 minutes at 37°C and imaged using EVOS FL Cell Imaging System in the red and green channels [126].

4.2.8.6 Assessment of intracellular ROS levels

To analyze the intracellular ROS levels in the cells treated with various formulations, DCFDA assay was performed [127]. The MDA-MB-231 cells were seeded in 12-well cell culture plate with 50000 viable cells. After the cells were allowed to adhere for 24 h, the cells are exposed to various treatments as mentioned in mitochondrial depolarization assay. The cells were incubated with the treatments for 24 h, the cells are treated with 10 μM DCFH-DA (2',7'-dichlorodihydrofluorescein diacetate and further incubated for 30 minutes in dark. The cells were then imaged using EVOS FL Cell Imaging System in the green channel.

4.2.8.7 Cell cycle analysis

CBT induces cell cycle arrest in the G2/M phase. Cell cycle analysis was performed to confirm whether the prepared CS-HA-Cmab-NP's anti-proliferative effect is due to the enhanced intracellular availability of CBT that subsequently increases the cell cycle arrest in the G2/M phase [128]. Briefly, in a 6-well plate, 1×10^6 MDA-MB-231 cells were seeded and allowed to adhere in incubation for 24 h. The cells were exposed to neat CBT, CS-HA-NP, and CS-HA-Cmab-NP at concentrations equal to IC_{50} of CS-HA-Cmab-NP for 24 h. The cells were harvested after 24 h using 1mM EDTA, then fixated using 80% ethanol and incubated overnight at -20°C. Subsequently, the cells were collected by centrifugation at 3000 rpm for 7 minutes. These cells were then incubated in a staining

buffer containing 0.1 mg/mL RNase A and 0.05 mg/mL propidium iodide in 0.1 % Triton X-100 in PBS and analyzed using flow cytometry.

4.2.9 In vivo studies in female Sprague Dawley rats

4.2.9.1 Pharmacokinetic assessment

To assess the pharmacokinetic profile of CS-HA-NP and CS-HA-Cmab-NP, healthy female Sprague Dawley rats were divided into three groups of 12 animals (n=12). Group 1 received CBT at a dose of 6.5 mg/kg via. tail vein. Groups 2 and 3 received CS-HA-NP and CS-HA-Cmab-NP equivalent to 6.5 mg/kg of CBT via. tail vein. Following the treatments, blood samples (0.5 mL) were taken from the orbital vein in heparinized tubes at the predetermined time points of 0.5, 1, 2, 3, 4, 6, 12, 18, 24, and 48 h. Blood samples were centrifuged at 6000 rpm for 10 min to isolate the plasma, kept at -80 ℃ until HPLC analysis was performed. The calibration curves in acetonitrile and plasma were prepared and validated. The plasma CBT concentration-time profile was plotted to determine the standard pharmacokinetic parameters using a non-compartmental model [129].

4.2.9.2 Tumor regression analysis and Histological assessment

DMBA-induced breast cancer model was used to evaluate the *in vivo* anti-tumor efficacy of the prepared nanoparticle [130]. To develop a breast cancer model, post-weaning pre-pubescent (5 weeks old) female Sprague Dawley rats were acclimatized for seven days. DMBA (65 mg/kg) dissolved in corn oil was subcutaneously injected into the breast pads of the acclimatized rats. After 10-12 weeks, the animals with an average tumor diameter of 10±1 mm were divided into four groups (n=5). Group 1 was designated as the control group, while Groups 2, 3, and 4 received neat CBT, CS-HA-NP, and CS-HA-Cmab-NP at a dose equivalent to 6.5 mg/kg twice a week for three weeks, respectively. The change in tumor volume and weight was monitored throughout the treatment period. On day 21, all

the animals were euthanized, and tissues were collected for histological assessment. Tissues from major organs were observed for signs of toxicity, while mammary tissue was assessed for progression of tumor. The tissues were stained with hematoxylin and eosin and observed under light microscope.

4.2.9.3 Survival study

To determine the survival rate of tumor-bearing rats receiving treatment, the rats were divided into five groups (n=5). Group one consisted of control healthy rats (n=5). Groups 2-5 consisted of tumor-bearing rats. Groups 1 and 2 received saline via. tail vein, while groups 3, 4, and 5 received neat CBT, CS-HA-NP, and CS-HA-Cmab-NP, respectively. The dose and frequency of the treatment were the same as described in the tumor regression study. The rats were housed for a maximum of 120 days. The individual death count was recorded throughout the observation period, and the Kaplan-Mier survival plot was obtained to determine the mean survival rate of each treatment group.

4.2.10 Statistics

The measurements were done in triplicates and data were presented as Mean±SD. The statistical variance among groups was determined by one-way and two-way ANOVA at p value <0.5 (*), 0.01 (**), 0.001 (***), and 0.0001 (****). The statistical analysis was performed using GraphPad Prism version 9.0.

4.3 Results and Discussion

4.3.1 Characterization of succinylated TPGS

The conjugated TPGS (succinylated TPGS; shown in **Figure 4.3**) was analyzed using FTIR. FTIR spectra (**Figure 4.4**) show an increased transmittance at -C=O stretch 1734 cm^{-1}, 1281 cm^{-1}, 1101 cm^{-1}, and 1059 cm^{-1} in TPGS-COOH indicating the possibility of the formation of another ester linkage. Also, the TPGS-COOH spectrum shows a broader

O-H stretch in the range of 3300-2800 cm^{-1} in comparison to TPGS, indicating the presence of a free carboxylic acid group.

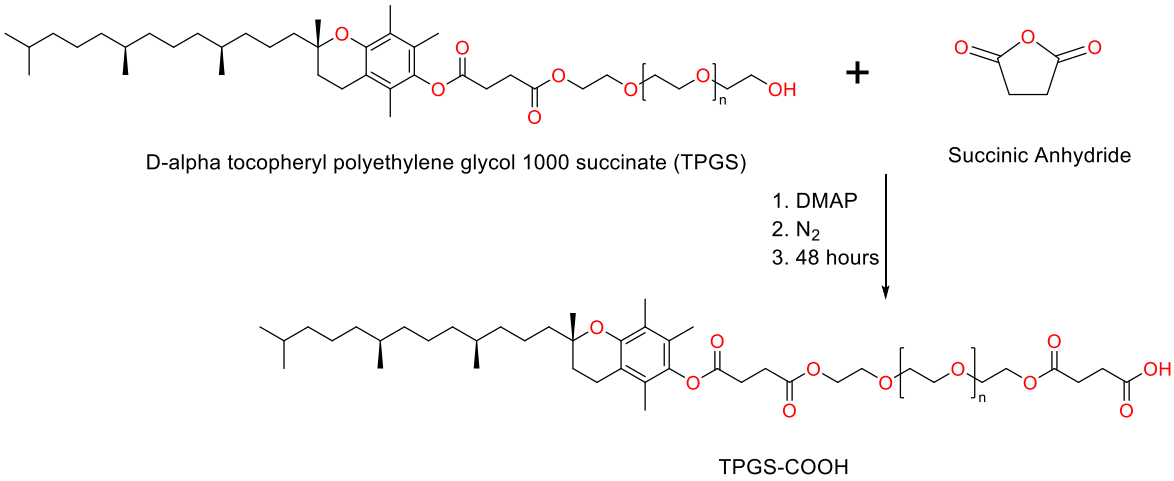

Figure 4.3 Succinylation of TPGS

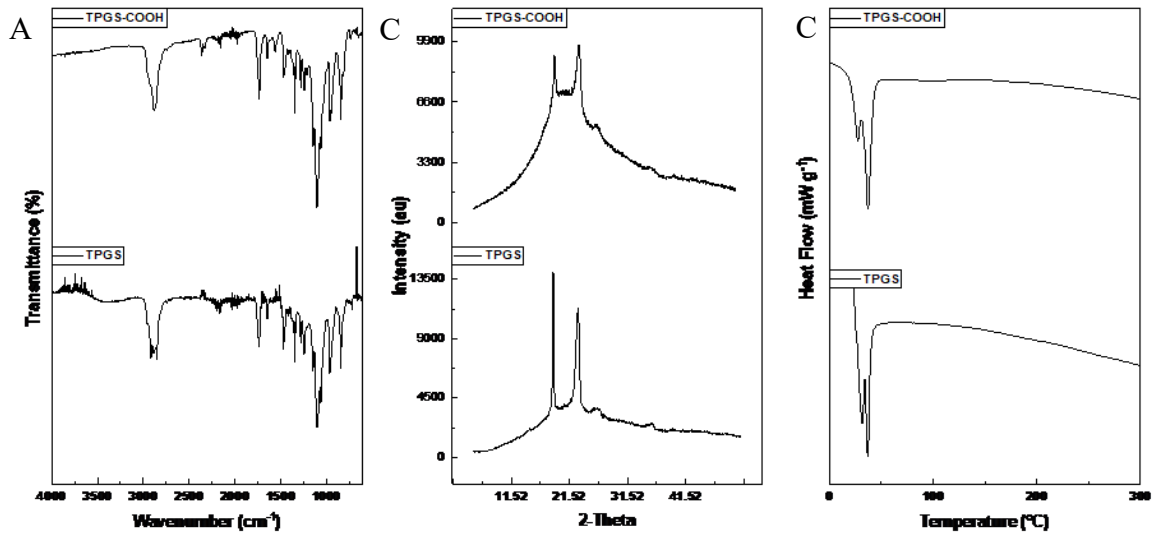

Figure 4.4 (A) FTIR, **(B)** DSC, and **(C)** XRD spectra of TPGS and TPGS-COOH

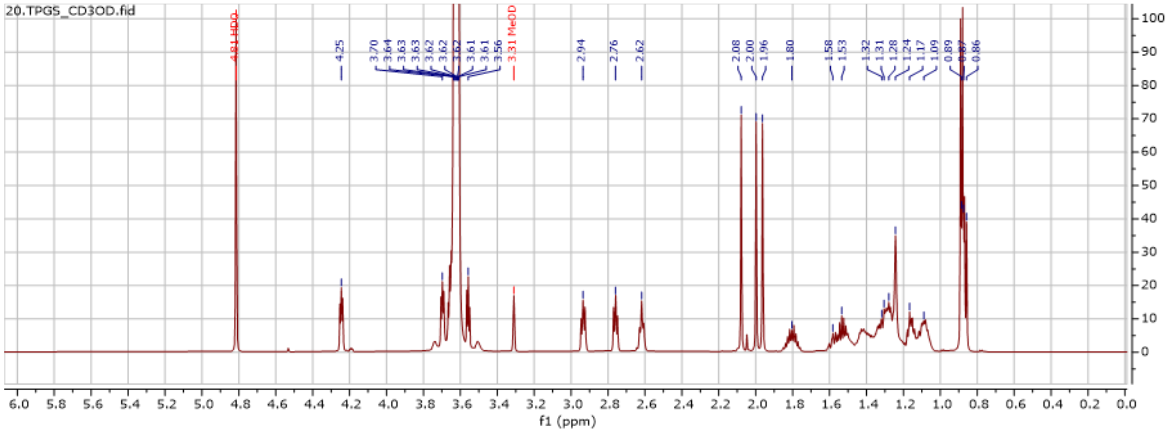

Figure 4.5 ^{1}H NMR spectrum of TPGS Deuterated Methanol.

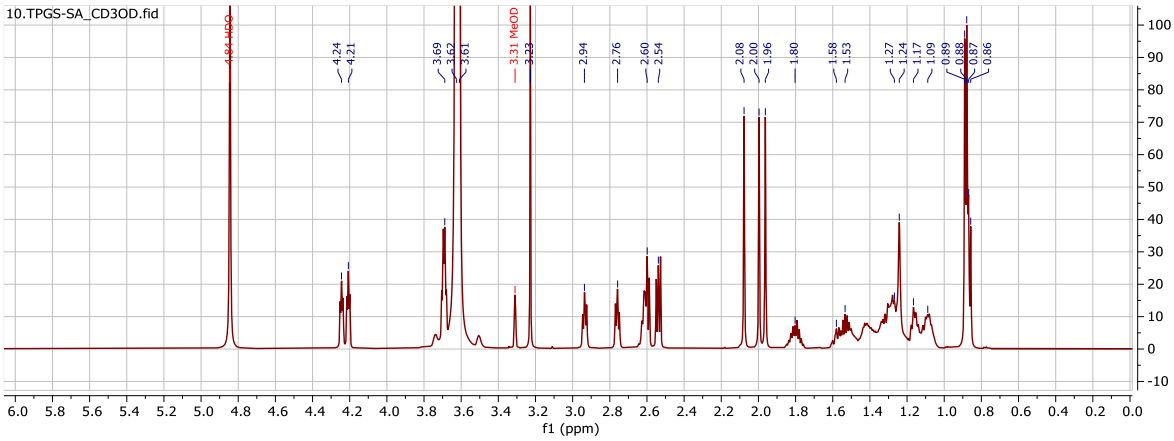

Figure 4.6 ^{1}H NMR spectrum of TPGS-COOH Deuterated Methanol.

Table 4.2 Interpretation of ^{1}H NMR Spectra of TPGS and TPGS-COOH

S. No	Proton	Chemical Shift (δ) ppm	
		TPGS	TPGS-COOH
1.	H1-H18	0.89-1.80	0.88-1.80
2.	H19-H22	2.00-2.08	1.80-2.08
3.	H23	2.62	2.60

4.	H24	2.76	2.76
5.	H25	4.25	4.24
6.	H26	2.94	2.94
7.	H27* -[C**H**$_2$-CH$_2$-O]$_n$-	3.62	3.61
8.	H28*-[CH$_2$-C**H**$_2$-O]$_n$-	3.63	3.62
9.	**H29**	**3.56**	**3.69**
10.	**H30**	**3.70**	**4.21**
11.	**H31**	--	**2.54**
12.	**H32**	--	**3.23**

NMR spectroscopy was performed for TPGS and TPGS-COOH samples dissolved in deuterated methanol (CD_3OD) to confirm the conjugation. The ^1H NMR spectra of TPGS and TPGS-COOH are as shown in **Figure 4.5** & **Figure 4.6** and detail characteristic peaks are in **Table 4.2**. The alkyl chain of the TPGS structure was in the range of 0.85 to 1.6 (H1-H16), followed by protons (H17-H22) of dihydrochromen unit of TPGS in the range of 1.7 ppm to 2.1 ppm. Meanwhile, the peaks in the 2.5 ppm to 4.3 ppm range were from the succinate ester and polyethylene glycol blocks [131]. After succinylation, TPGS-COOH showed an addition of two proton peaks (H31 and H32) in the range of 2.00 ppm to 3.50 ppm and a downfield shift in proton signals from the terminal polyethylene (H29 and H30) block of TPGS indicating the successful conjugation of succinic anhydride to TPGS via. esterification [132]. The ^{13}C NMR spectra were also in agreement with ^1H NMR, as the conjugation of succinic anhydride resulted in 4 new carbon signals (C40-C43). The appearance of two distinct peaks in the 170-180 ppm range (C40 and C43) is due to the carbonyl carbon forming ester linkage with the terminal hydroxyl group of

TPGS and a free terminal carboxylic acid group. The α and β carbon of the succinyl group are the other two peaks (C41 and C42) appearing in the 28-30 ppm range. Details in (**Table 4.3**, **Figure 4.7**& **Figure 4.8**).

Table 4.3 Interpretation of ^{13}C NMR Spectra of TPGS and TPGS-COOH

S. No	Carbon	Chemical Shift (δ) ppm	
		TPGS	TPGS-COOH
1.	C1-C2	20.19	20.19
2.	C3, C7, and C11	27.78	27.78
3.	C4	39.18	39.18
4.	C5, C9, and C13	24.10	24.10
5.	C6, C8, C10, C12, and C14	37.02	37.03
6.	C15 and C16	18.90	18.92
7.	C17	24.55	24.55
8.	C18	74.79	74.80
9.	C19	32.57	32.57
10.	C20	21.72	21.74
11.	C21-C26	117-150	117-150
12.	C27-C29	10.75-11.89	10.77-11.92
13.	C30 and C33	171.51 and 172. 49	171.51 and 172.49
14.	C31 and C32	28.47 and 28.29	28.47 and 28.30
15.	C34 and C35	63.63 and 68.70	63.64 and 68.71

16.	C36 and C37	70.21 and 70.04	70.19 and 70.11
17.	C38 and C39	72.32 and 60.87	68.71 and 63.41
18.	**C40 and C43**	--	**176.22 and 177.03**
19.	**C41 and C42**	--	**29.90 and 29.37**

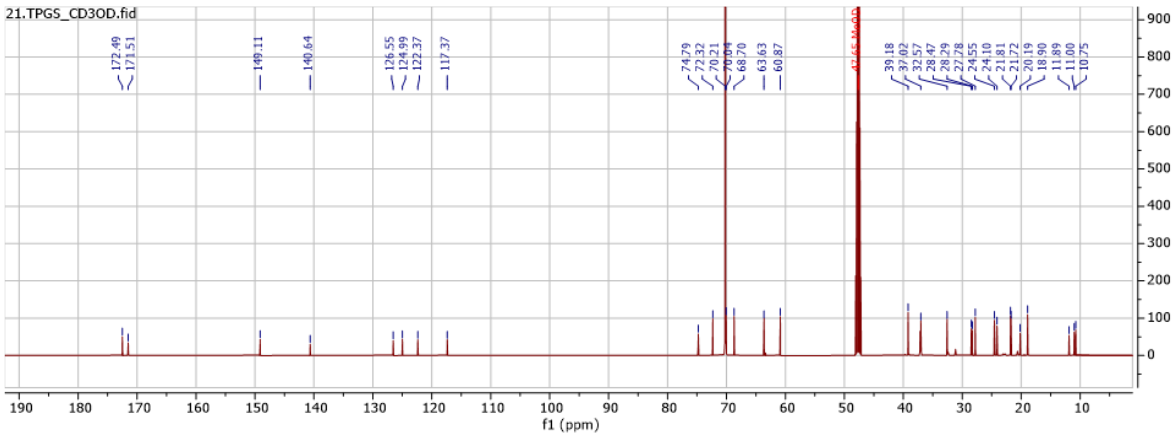

Figure 4.7 ^{13}C NMR spectrum of TPGS Deuterated Methanol.

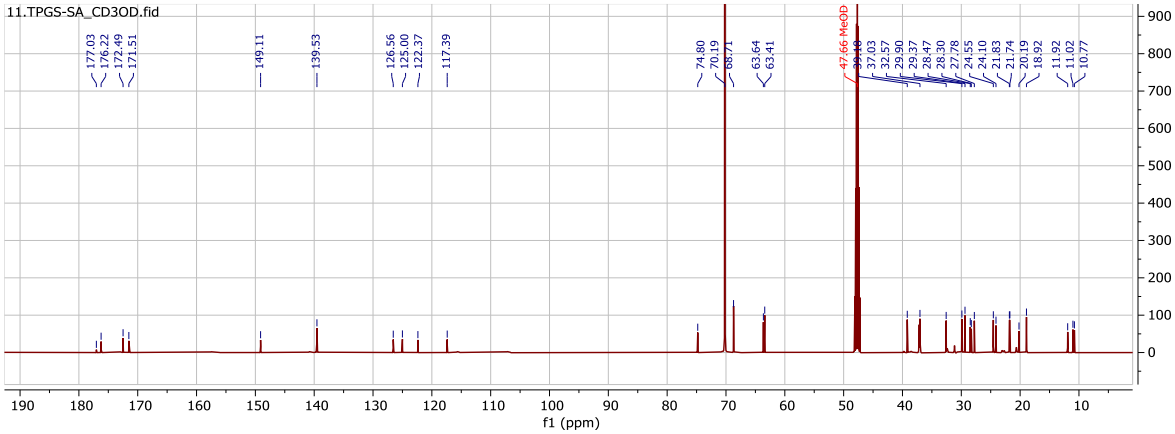

Figure 4.8 ^{13}C NMR spectrum of TPGS-COOH in Deuterated Methanol.

The conjugation was further confirmed with mass spectroscopy [133]. Mass fragment values of TPGS and TPGS-COOH are given in **Figure 4.9** to **Figure 4.12** and **Table 4.4**. Fragments 164.9, 431.5, and 531.5 are standard fragments of D-α-tocopheryl succinate. The peaks at 663.9, 751.6, 795.6, 839.4, 1323.6, 883.7, 927.6, 971.4, 1015.6, 1059.6,

1103.6, 1147.6, 1191.6, 1235.5, 1279.7, 1367.7, 1411.6, 1455.6, 1499.7, 1543.6, 1587.6, 1631.7, 1675.6, 1719.6, 1763.5, and 1807.6 are due to the fragmentation of polyethylene blocks (OC_2H_4) with a reduction of ~44 Da (or multiples of 44) molecular weight [134,135]. The highest molecular weight of the TPGS was observed at 1807 Da, with a molecular ion peak at 1807.9 (M+1). However, the average molecular weight for the sample was ~1543 Da. The peaks observed at 635.6, 723.5, 767.6, 811.6, 855.5, 899.8, 943.5, 987.6, 1031.6, 1075.6, 1119.6, and 1163.5, corresponding to the subsequent fragmentation of 663.9, 751.6, 795.6, 839.4, 1323.6, 883.7, 927.6, 971.4, 1015.6, 1059.6, 1103.6, 1147.6, and 1191.6 fragments with the loss of (C_2H_4, m/z=28 Da). In the case of TPGS-COOH, a fragmentation pattern similar to TPGS was observed. Moreover, additional fragments were observed at 1203.4, 1247.7, 1291.5, 1335.7, 1379.7, 1423.9, 1467.7, 1511.6, 1555.7, 1599.6, 1643.6, 1687.7, 1731.7, 1775.6, 1819.5, 1863.5, and 1907.7. These fragments were molecular ion peaks (M+1) of succinylated TPGS that showed an increment of ~100 Da in the TPGS fragments observed at 1103.6, 1147.6, 1191.6, 1235.5, 1279.7, 1367.7, 1411.6, 1455.6, 1499.7, 1543.6, 1587.6, 1631.7, 1675.6, 1719.6, 1763.5, and 1807.6 due to the conjugation of succinic anhydride (MW ~101Da). The smallest molecular ion peak of TPGS-COOH at 1203.4 may also indicate that the 1103.603 fragment was the smallest molecular ion peak of TPGS (M+1). This suggests that the molecular weight range of the TPGS sample was 1102-1806 Da.

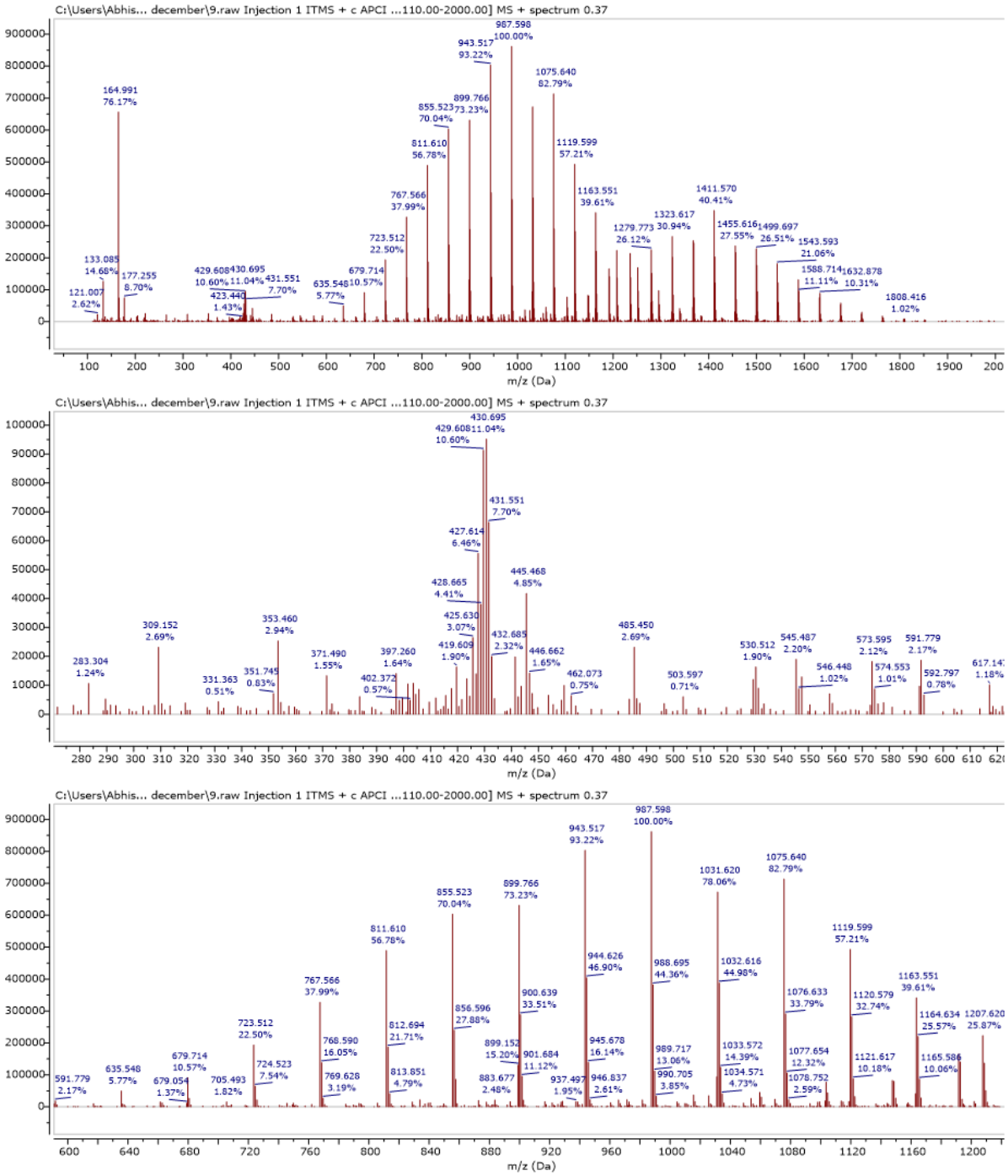

Figure 4.9 Mass spectra of TPGS at {m/z (Da) = 300-1200}

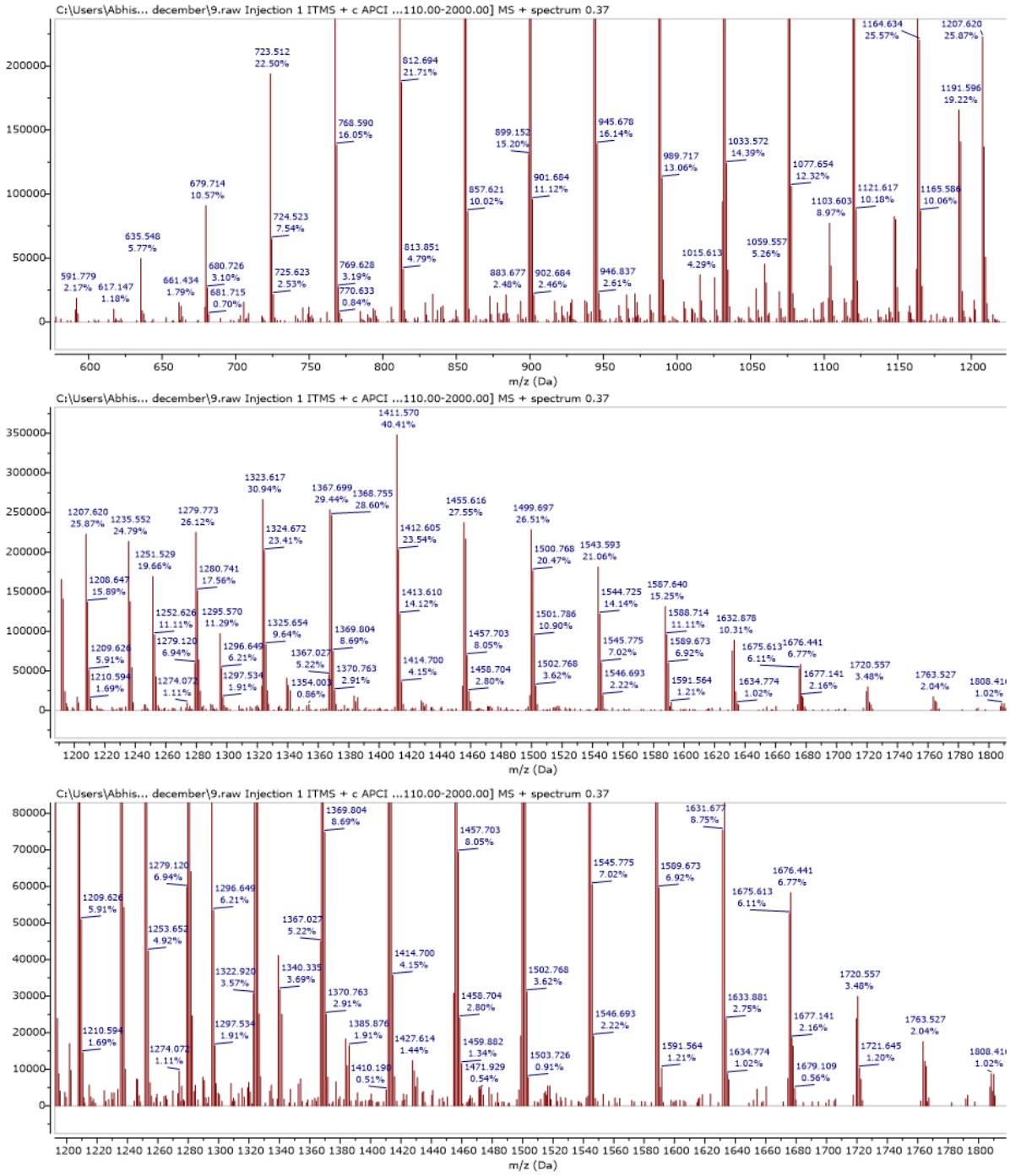

Figure 4.10 Mass spectra of TPGS at {m/z (Da) = 600-1800}

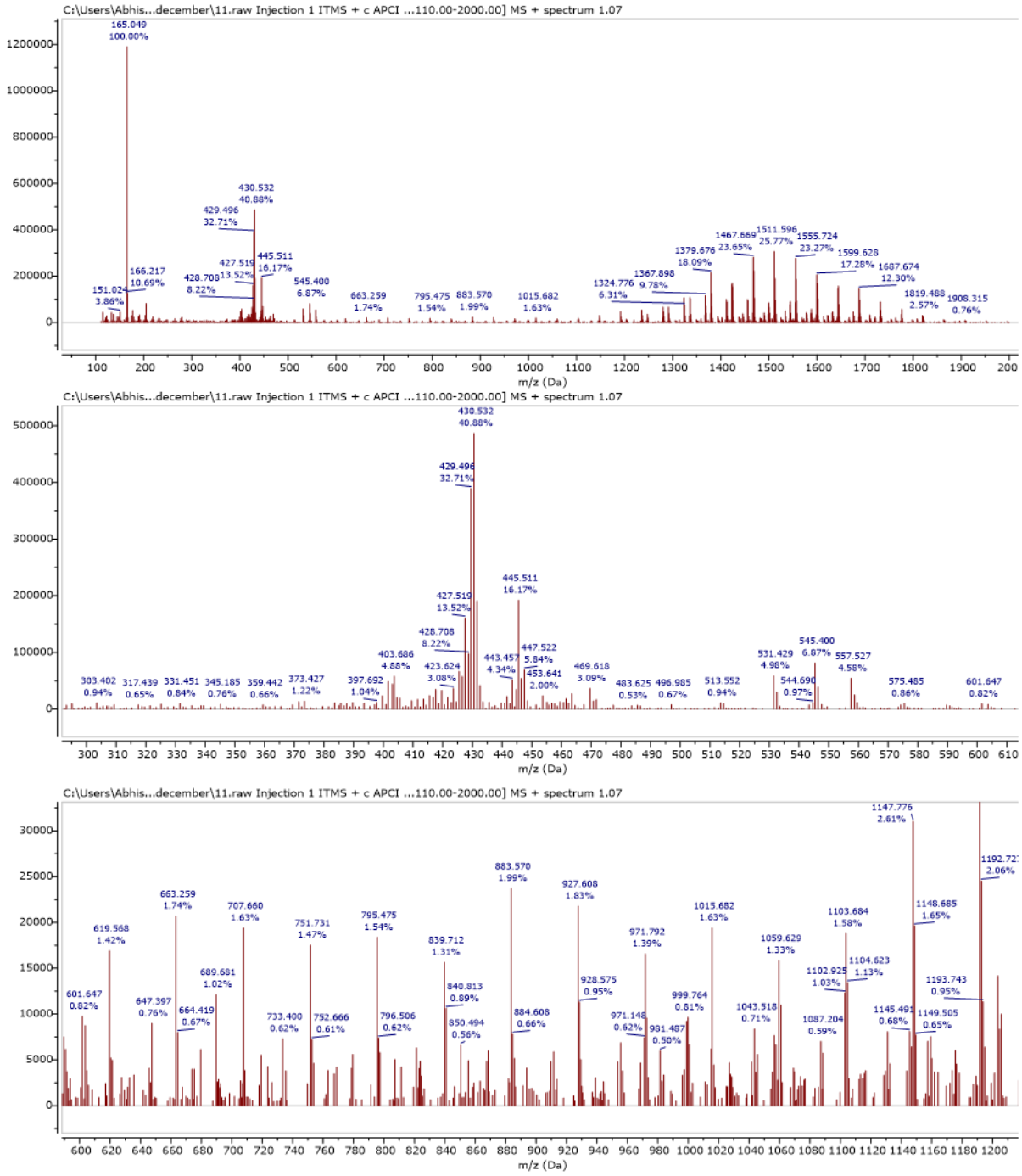

Figure 4.11 Mass spectra of TPGS-COOH at m/z (Da) in the range of 300-1200

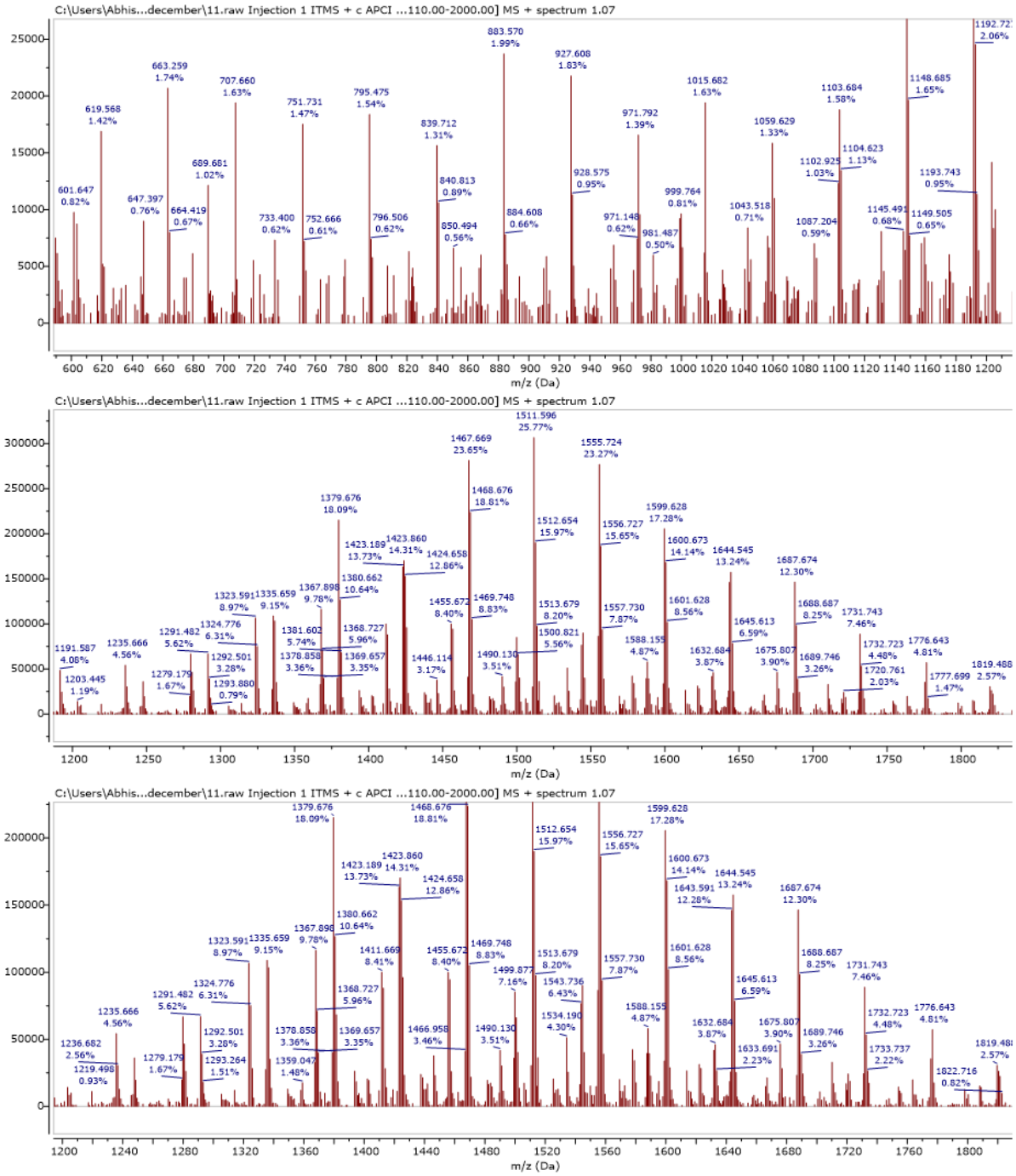

Figure 4.12 Mass spectra of TPGS-COOH at m/z (Da) in the range of 600-1800

Table 4.4 Interpretation of the mass (TOF) spectra of TPGS and TPGS-COOH

S. NO.	MASS FRAGMENTS OF TPGS AND TPGS-COOH			
	TPGS (C_2H_4) fragments	**TPGS (OC_2H_4) fragments**	**TPGS-COOH (OC_2H_4) fragments**	**TPGS-COOH Succinylated fragments (+100 Da)**
1.	--	164.991	165.049	
2.	--	431.551	431.544	
3.	--	531.468	531.429	
4.	***635.548***	663.922	663.259	
6.	***723.512***	751.620	751.731	
7	***767.566***	795.641	795.475	
8.	***811.610***	839.377	839.712	
9.	***855.523***	883.677	883.570	
10.	***899.766***	927.645	927.608	
11.	***943.517***	971.367	971.792	
12.	***987.598***	1015.613	1015.682	
13.	***1031.620***	1059.557	1059.629	
14.	***1075.640***	1103.603	1103.684	**1203.445**
15.	***1119.599***	1147.581	1147.776	**1247.711**
16.	***1163.551***	1191.596	1191.587	**1291.482**
17.	--	1235.552	1235.666	**1335.659**
18.	--	1279.773	1279.176	**1379.676**
19.	--	1323.617	1323.591	**1423.860**
20.	--	1367.699	1367.898	**1467.669**
21.		1411.570	1411.669	**1511.596**
22.		1455.616	1455.672	**1555.724**
23.		1499.697	1499.877	**1599.628**

24.	1543.593	1543.736	**1643.591**
25.	1587.640	1587.443	**1687.694**
26.	1631.677	1631.680	**1731.743**
27.	1675.613	1675.867	**1775.581**
28.	1719.638	1719.395	**1819.488**
29.	1763.527	1763.542	**1863.540**
30.	1807.558	1807.961	**1907.687**

4.3.2 Characterization of nanoparticles

The nanoparticles were prepared with modified ionic gelation (**Figure 4.1**) and were characterized for particle size, surface charge, polydispersity index, entrapment efficiency and drug loading (detail in **Table 4.5**). The hydrodynamic size determined using photon correlation spectroscopy (PCS) was found to be 157.01±13.44, 163.2±17.28, and 175.4±20.76 for bCS-HA-NP, CS-HA-NP, and CS-HA-Cmab-NP, respectively. The nanoparticles exhibited particle size and zeta potential close to previous reports for HA/CS nanoparticles [136]. An increase in the hydrodynamic size of the particles and decrease in zeta potential was observed due to the loading of cabazitaxel and subsequent surface conjugation of cetuximab. However, the change was not significant (P value > 0.05). The lower zeta potential observed for CS-HA-Cmab-NP than CS-HA-NP was attributed to the surface conjugation of Cmab [120]. The PDI of all the particles was found to be less than 0.3, indicating the formation of a monodispersed colloidal dispersion [137].

Morphological assessment was done using TEM, SEM, and AFM analysis **(Figure 4.13)**. 2D image acquired using TEM revealed round nanoparticles in the sub-200 nm range. CS-HA-NP and CS-HA-Cmab-NP were found to be 108.82±25.31 nm and 127.28±9.79 nm average size, respectively. SEM micrograph provided 3D images of CS-HA-NP and

CS-HA-Cmab-NP. The particles appeared monodispersed and spherical. The average size of CS-HA-NP and CS-HA-Cmab-NP were 116.17±15.53 nm and 131.55±18.04 nm, respectively. The AFM analysis also revealed the smooth surface of the prepared nanoparticles and was in agreement with TEM and SEM analysis. The lower particle size observed in electron microscopy compared to PCS is because PCS measures the hydrodynamic diameter of the particles still dispersed in a media [138]. In contrast, electron microscopy is done on dried samples.

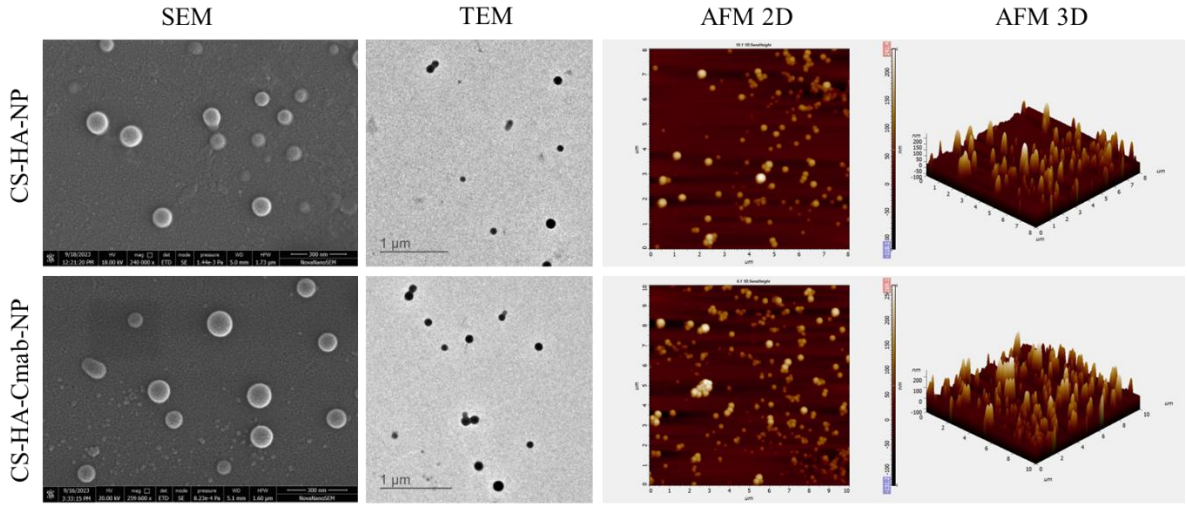

Figure 4.13 Morphological assessment of CS-HA-NP and CS-HA-Cmab-NP by TEM, SEM and AFM.

Table 4.5 Characterization of CS-HA-NP and CS-HA-Cmab-NP nanoparticles

Batch Code	Particle size (nm)			Zeta potential (mV)	PDI	CBT		C6		CTX
	DLS/PC	SEM	TEM			EE (%)	DL (%)	EE (%)	DL (%)	Degree of conjugation
bCS-HA-NP	157.01±13.44	--	--	25.08±1.46	0.228	--	--	--	--	--
CS-HA-NP	163.2±17.28	116.17±15.53	108.82±25.31	23.85±2.07	0.266	76.53±2.42	4.29±0.52	--	--	--
CS-HA-Cmab-NP	175.4±20.76	131.55±18.04	127.28±9.79	19.28±2.15	0.293	75.44±2.67	4.11±0.41	--	--	81.52±3.71
c6CS-HA-NP	166.27±18.02	--	--	24.41±1.80	0.267	74.06±1.91	4.18±0.39	95.27±3.28	0.18±0.01	--
c6CS-HA-Cmab-NP	187.3±15.28	--	--	19.17±2.33	0.238	73.89±2.05	4.01±0.45	94.18±4.77	0.17±0.01	81.64±3.53

Data presented as Mean ± SD

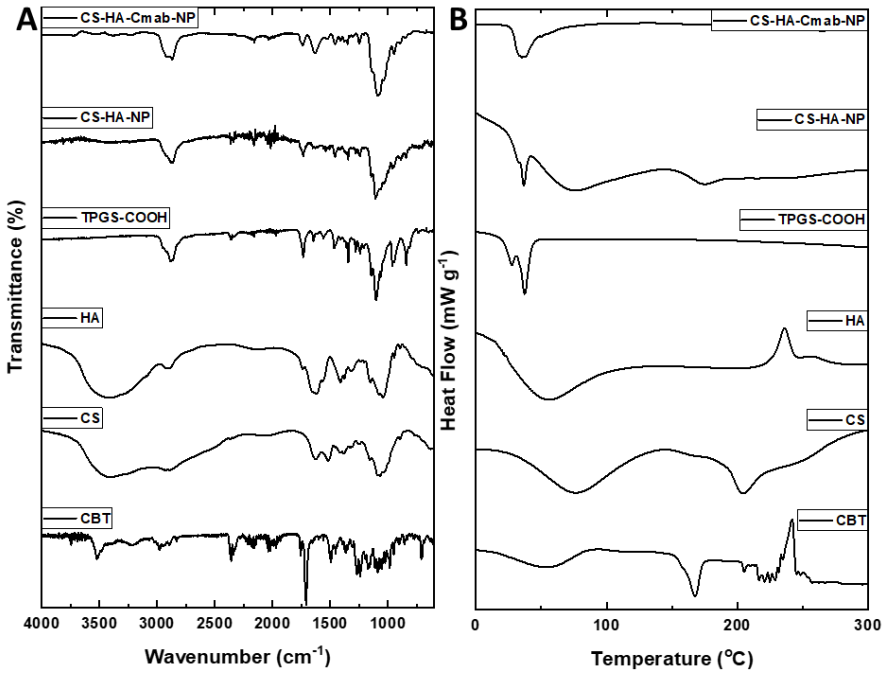

Figure 4.14 (A) FTIR and **(B)** DSC spectra of neat CBT, CS, HA, TPGS-COOH, CS-HA-NP, and CS-HA-Cmab-NP.

4.3.2.1 Solid-state characterization of nanoparticles

FTIR spectra of neat CBT, CS, HA, TPGS-COOH, CS-HA-NP and CS-HA-Cmab-NP are shown in **Figure 4.14 (A)**. The characteristic peaks of CBT were masked in CS-HA-NP and CS-HA-Cmab-NP attributed to drug encapsulation in nanoparticles. The peaks observed in nanoparticles were of polymer used in synthesis of nanoparticles. The neat CBT had an endothermic peak at 167 °C attributed to crystalline nature of drug. The coarse drug also showed an exothermic peak at 241 °C, indicating drug breakdown at higher temperature. Pure CS had two endothermic peaks at 75 °C and 204 °C, similar to previous report. While, pure HA was found to have an endothermic peak at 53 °C and an exothermic peak at 236 °C. The endothermic peak of TPGS-COOH was seen as a split dual peak at 27 °C and 37 °C. In contrast, nanoparticle CS-HA-NP showed peaks at 35 °C, 73 °C, and 174 °C, corresponding to TPGS-COOH, CS, and HA blend used in nanoparticles synthesis. While, a low intensity endothermic peak at 35 °C was observed

for CS-HA-Cmab-NP corresponding to TPGS. The decrease in intensity might be due to Cmab conjugation with TPGS-COOH for surface modification of nanoparticles **Figure 4.14 (B).**

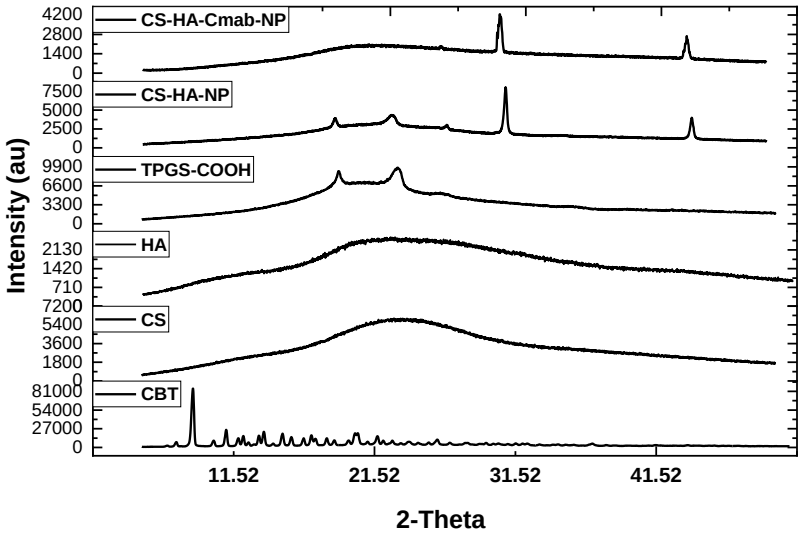

Figure 4.15 XRD spectra of neat CBT, CS, HA, TPGS-COOH, CS-HA-NP, and CS-HA-Cmab-NP.

The XRD diffraction spectrum of coarse drug showed high intensity peaks, corresponding to crystalline drug. Whereas, CS and HA exhibited broad amorphous diffraction peak. The peaks of coarse drug were masked in nanoparticles, CS-HA-NP. This could be due to drug entrapment in polymeric nanoparticles core and the peaks were corresponding to TPGS-COOH, CS, and HA. A decrease in TPGS-COOH peaks intensity was observed probably due to Cmab conjugation on nanoparticles surface **Figure 4.15**.

4.3.2.2 Encapsulation efficiency, drug loading, degree of cetuximab conjugation and surface chemistry

The encapsulation efficiency (EE) estimated using HPLC was 76.53±2.42 % and 75.44±2.67 % for CS-HA-NP and CS-HA-Cmab-NP, respectively (Table 2). While the change in EE was not significant, the slightly lower encapsulation may be attributed to

the conjugation process. The drug loading was determined as the percentage weight of CBT in the purified and washed nanoparticles, which was found to be 4.29±0.52 % for CS-HA-NP and 4.11±0.41 % for CS-HA-Cmab-NP. Bradford's assay was successfully performed to confirm the conjugation of Cmab on the nanoparticle surface. Bradford's assay is a colorimetric method to estimate the protein content in a sample. Quantitative estimation of Cmab, using BSA as a standard, was done to calculate the amount of protein conjugated on the surface of freshly prepared nanoparticles [139]. The results showed that the protein content in the washed CS-HA-Cmab-NP sample was 1.63 mg (108.66 µg/mL), to which 2 mg of Cmab was initially added, making the degree of conjugation of Cmab to CS-HA-Cmab-NP 81.5%. To further confirm the conjugation, the surface composition of CS-HA-NP and CS-HA-Cmab-NP was assessed using XPS. XPS spectra also showed change in surface composition of nanoparticles post conjugation of Cmab on its surface. The atomic percentage of nitrogen showed a significant increase from 3.53% in CS-HA-NP to 7.74% in CS-HA-Cmab-NP, while phosphorus exhibited a marked reduction from 1.42% in CS-HA-NP to 1.07% in CS-HA-Cmab-NP. Also, a sulfur peak was observed in CS-HA—CmabNP (0.13%). The increase in nitrogen percentage and presence of sulfur indicates that the surface composition of CS-HA-Cmab-NP has changed due to the conjugation of Cmab (**Table 4.6**). Besides, the crosslinker used in the ionic gelation of nanoparticles results in the presence of a phosphorus peak, which is evidently diminished in the case of CS-HA-Cmab-NP, indicating that the surface of the nanoparticle is functionalized with Cmab. The XPS spectra of CS-HA-NP and CS-HA-Cmab-NP are shown in **Figure 4.16**.

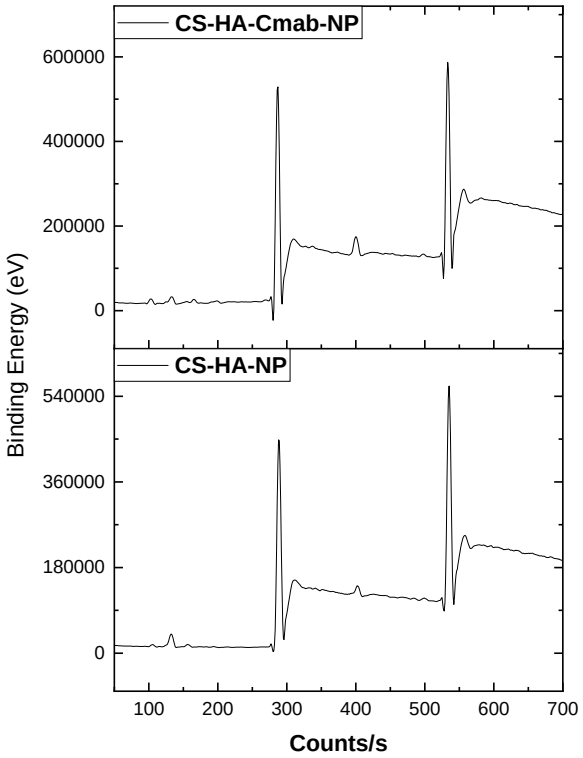

Figure 4.16 XPS spectra of CS-HA-NP and CS-HA-Cmab-NP.

Table 4.6 XPS surface atomic percentage of N1s, O1s, C1s, S2p, and P2p in CS-HA-NP and CS-HA-Cmab-NP

S. No.	Formulation code	Atomic percentage (%)				
		N 1s	O 1s	C 1s	S2p	P2p
1	CS-HA-NP	3.53	31.15	63.89	0.01	1.42
2	CS-HA-Cmab-NP	7.74	30.36	60.71	0.13	1.07

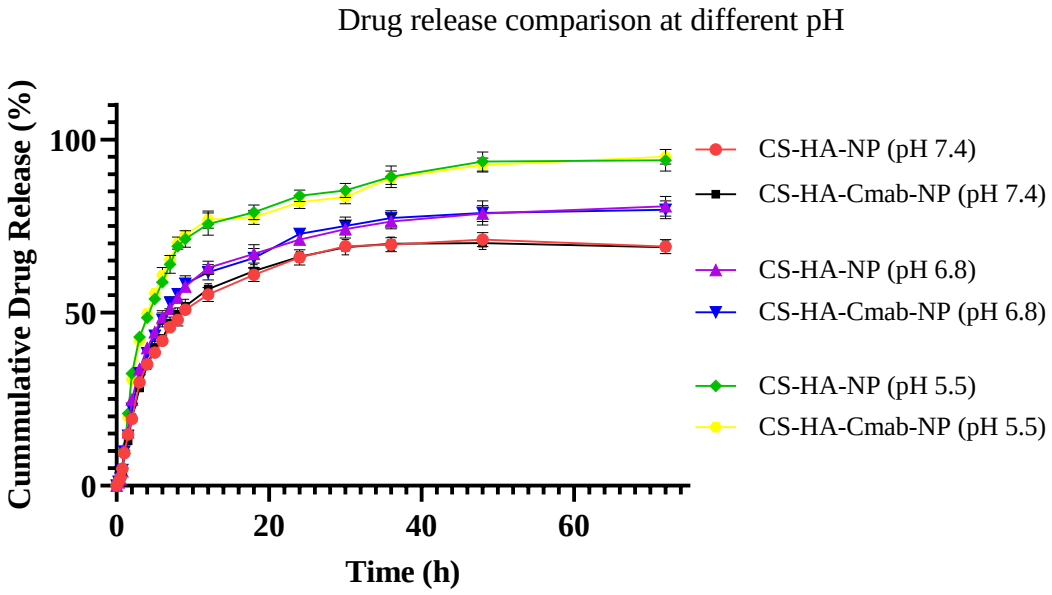

Figure 4.17 The drug release profile of CS-HA-NP and CS-HA-Cmab-NP in Phosphate Buffered Saline pH 7.4, Phosphate Buffer pH 6.8, and Acetate Buffer pH 5.5. Comparative graph of release profiles of CS-HA-NP and CS-HA-Cmab-NP at various pH. Data presented as Mean ± SD (vertical bars); n=6.

4.3.3 Drug release study

The dialysis (MWCO 1000 Da) method was used to determine the drug release profile of nanoparticles at pH 7.4, 6.8 and 5.5 (**Figure 4.17**). In PBS pH 7.4, CS-HA-NP showed 41.8±1.1%, 55.2±2.0%, and 65.9±2.3% drug release at 6, 12, and 24 h. Similarly, CS-HA-Cmab-NP showed 42.5±1.3%, 56.7±1.6%, and 66.1±1.5% drug release at 6, 12, and 24 h, respectively. However, the extent and rate of drug release significantly increased with lower pH. For instance, CS-HA-Cmab-NP in pH 6.8 phosphate buffer, exhibited an 11.3%, 10.9%, and 11.0% increase in the extent of drug release at 6, 12, and 24 h, respectively as compared to PBS pH 7.4. The percentage release in pH 5.5 acetate buffer

was 14.3%, 13.6%, and 12.4% higher than release observed in PBS pH 7.4 at 6, 12, and 24h. A similar trend was also observed in the case of CS-HA-NP. Also, at pH 5.5, more than 94% of the drug was released from nanoparticles, while in pH 7.4 PBS, the maximum amount of drug release was below 70%.

The results indicate a significant (****p value <0.0001) increase in the rate and extent of drug release with a decrease in pH. This may be attributed to the pH-responsive nature of the CS, as it protonates at lower pH and exhibits swelling behavior. This swelling behavior and its role in drug release is also evident with the release kinetics that suggests that the nanoparticles follow the Weibull and Gompertz model for drug release (details in **Table 4.7**). These models primarily indicate swelling and diffusion-dependent drug release from the system [140–142].

Table 4.7 Correlation coefficients of Cabazitaxel release profile from CS-HA-NP and CS-HA-Cmab-NP at various pH in various fitted release kinetic models

Model	Parameter	CS-HA NP (pH 7.4)	CS-HA-Cmab NP (pH 7.4)	CS-HA NP (pH 6.8)	CS-HA-Cmab NP (pH 6.8)	CS-HA NP (pH 5.5)	CS-HA-Cmab NP (pH 5.5)
Zero-order	**r^2**	0.9570	0.9697	0.9547	0.9678	0.9392	0.9578
First Order	**r^2**	0.9815	0.9859	0.9782	0.9842	0.9699	0.9755
Higuchi	**r^2**	0.8785	0.8675	0.8664	0.8635	0.8593	0.8537
Korsemeyer –Peppas	**r^2**	0.9737	0.9786	0.9679	0.9762	0.9553	0.9662
Hixson Crowell	**r^2**	0.9763	0.9834	0.9744	0.9824	0.9668	0.9765
Hofenberg	**r^2**	0.9814	0.9859	0.9782	0.9842	0.9699	0.9768
Baker-Lonsdale	**r^2**	0.8587	0.8464	0.8426	0.8395	0.8293	0.8210
Makoid	**r^2**	0.9978	0.9978	0.9937	0.9967	0.9913	0.9949

Bankar							
Peppas	**r^2**	0.9899	0.9917	0.9874	0.9907	0.9804	0.9857
Sahlin							
Quadratic	**r^2**	0.9876	0.9880	0.9813	0.9857	0.9732	0.9782
Model							
Weibull	**r^2**	0.9940	0.9951	0.9957	0.9958	0.9945	0.9965
Model	**β**	0.733	0.787	0.655	0.718	0.666	0.739
	AIC	35.8584	34.0797	35.6696	34.8016	42.9422	38.6233
	MSC	1.8869	1.6052	1.8548	1.7141	3.5928	2.4262
Logistic	**r^2**	0.9879	0.9912	0.9856	0.9910	0.9825	0.9902
Model	**β**	2.580	2.714	2.782	2.840	3.064	3.253
	AIC	41.6236	38.4950	46.9820	41.2105	53.7530	47.8925
	MSC	3.9152	4.2418	3.7468	4.2178	3.5531	4.1395
Gompertz	**r^2**	0.9972	0.9976	0.9962	0.9981	0.9955	0.9985
Model	**β**	1.342	1.409	1.527	1.537	1.833	1.947
	AIC	25.6308	24.0075	32.4041	24.3507	38.8934	27.1878
	MSC	5.3691	5.5588	5.0721	5.7505	4.9040	6.0218

4.3.4 In vitro assessment of nanoparticle efficacy

4.3.4.1 MTT assay

Cell viability assay was performed on MDA-MB-231 (**Figure 4.18**). The cells were exposed to neat CBT, bCS-HA-NP, CS-HA-NP, and CS-HA-Cmab-NP at various concentrations for 24 h. The assay revealed IC_{50} value of neat CBT, bCS-HA-NP, CS-HA-NP, and CS-HA-Cmab-NP to be 3.521±0.213, 2.064±0.093, and 1.462±0.079 µg/mL, respectively. The IC_{50} value suggests that CS-HA-Cmab-NP was 2.41-fold and 1.71-fold more toxic than neat CBT and CS-HA-NP respectively. This significantly improved

cytotoxicity may be attributed to the small sub-micron size of the prepared particles, their ability to undergo cellular uptake, and improve the intracellular concentration of CBT.

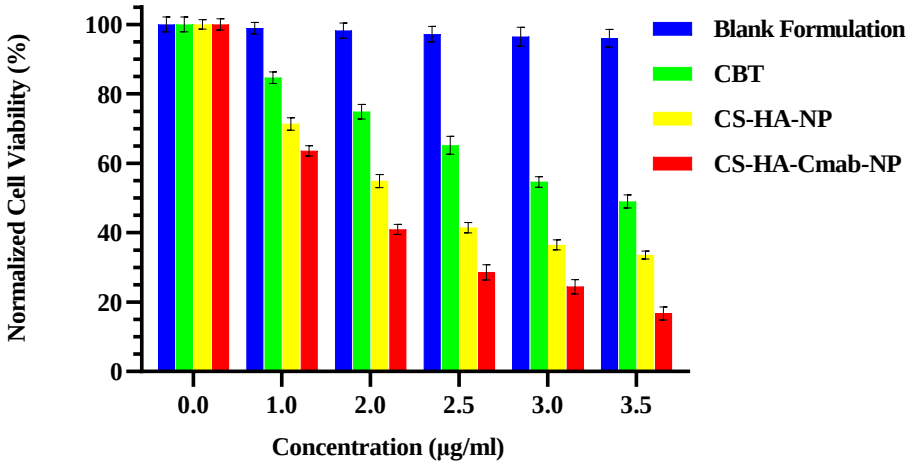

Figure 4.18 Normalized cell viability of bCS-HA-NP, Neat CBT, CS-HA-NP, and CS-HA-Cmab-NP at various concentrations calculated by MTT assay. Data presented as Mean ± SD (vertical bars); n=6.

4.3.4.2 Cellular uptake study

A qualitative cellular uptake study was performed to determine whether the improved efficacy against the MDA-MB-231 is due to the ability of nanoparticles to enhance the intracellular accumulation of CBT. After 6 h of exposure to free C6, c6CS-HA-NP, and c6CS-HA-Cmab-NP, the cells were imaged using a fluorescence microscope. The c6CS-HA-Cmab-NP treated cells gave the most intense signal of C6 followed by c6CS-HA-NP, indicating higher intracellular accumulation of payload in nanoparticle-treated cells. The cells treated with free C6 showed the least cellular uptake (**Figure 4.19**). Also, to assess if EGFR facilitated the cellular uptake of c6CS-HA-Cmab-NP via. receptor-mediated endocytosis, cells were pretreated with Cmab and then subsequently exposed to c6CS-HA-Cmab-NP. The pretreated cells showed a marked decline in the intracellular fluorescent signals of c6 in comparison to c6CS-HA-Cmab-NP, indicating that Cmab

conjugated on the surface of c6CS-HA-Cmab-NP facilitates their higher accumulation via. receptor-mediated endocytosis.

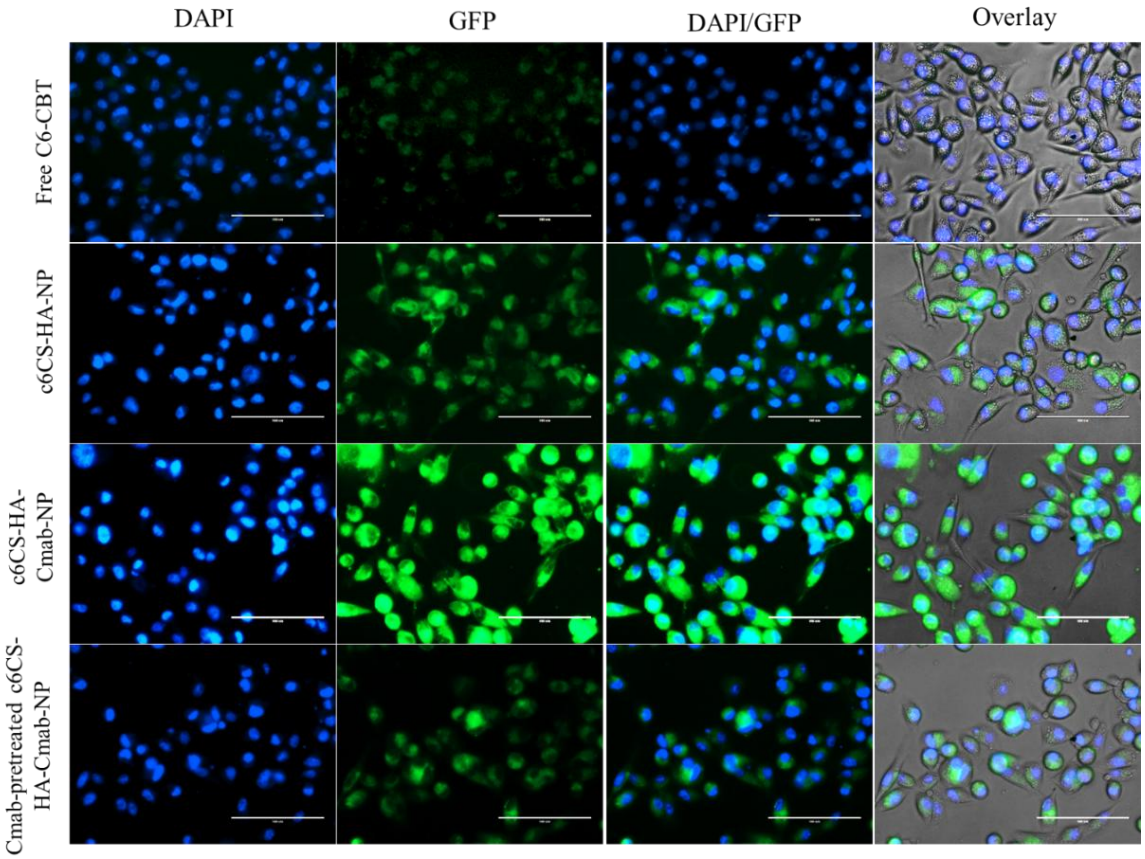

Figure 4.19 Microscopic images of cells imaged using fluorescence microscope after treatment with Free C6, c6CS-HA-NP, and c6CS-HA-Cmab-NP for 6 h. Cells were counter stained with DAPI. Scale bar = 100 µm.

4.3.4.3 Hoescht PI staining

The nuclear morphology of apoptotic cells can be assessed using Hoechst-PI staining. Hoechst33342, a cell permeable dye that binds to the adenine-thymine rich regions of DNA and emits blue fluorescence. The condensation of chromatin network in apoptotic cells induces a brighter blue fluorescent signal allowing the differentiation of pycnotic nuclei of apoptotic cells from healthy nuclei with diffused fluorescent signals. Propidium Iodide (PI), however is not permeable in viable cells and only stains the DNA of cells

with loss of membrane integrity, i.e. dead cells and cells at late apoptosis stage. The control and bCS-HA-NP treated cells showed low intensity diffused blue fluorescence with no permeation of PI indicating normal cells with intact plasma membrane **(Figure 4.20)**.

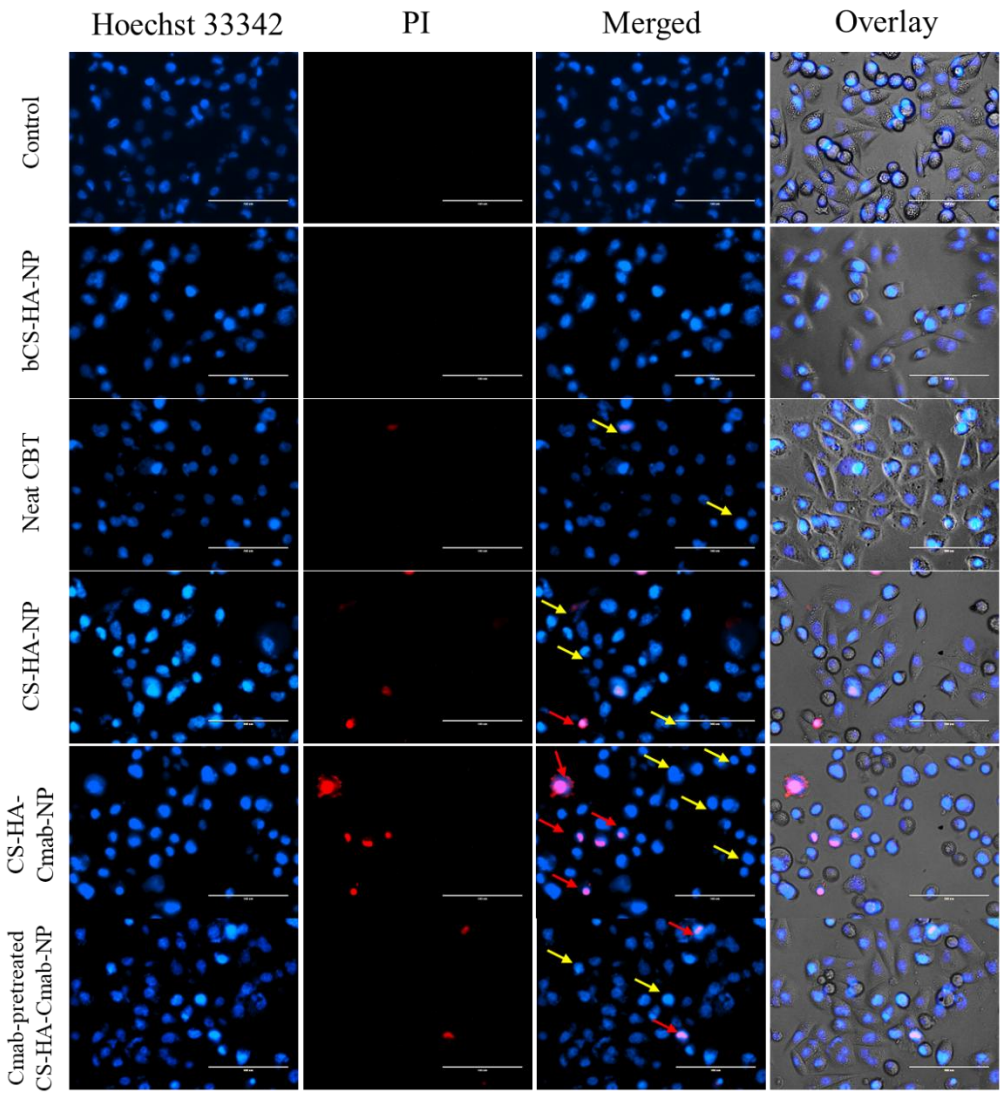

Figure 4.20 Hoechst33342/PI-stained MDA-MB-231 cells after 24 h treatment with Neat CBT, bCS-HA-NP, CS-HA-NP, CS-HA-Cmab-NP. The yellow and red arrows represent early apoptotic and late apoptotic cells respectively. Cells emitting blue fluorescence are Hoechst positive while those with red fluorescence are PI positive. Scale bar= 100 µm.

However, the cell receiving neat CBT exhibited brighter blue signals and signs of PI permeation, indicating the induction of apoptosis and nuclear condensation. The intensity of blue fluorescence and extent of PI permeation showed a marked increase in the cells treated with nanoparticles, with the highest PI permeation observed in CS-HA-Cmab-NP treated cells. The Cmab pretreatment, however, resulted in lower PI permeation and more diffused blue fluorescent signals, suggesting that the intracellular accumulation of CBT was reduced due to the blocking of EGFR.

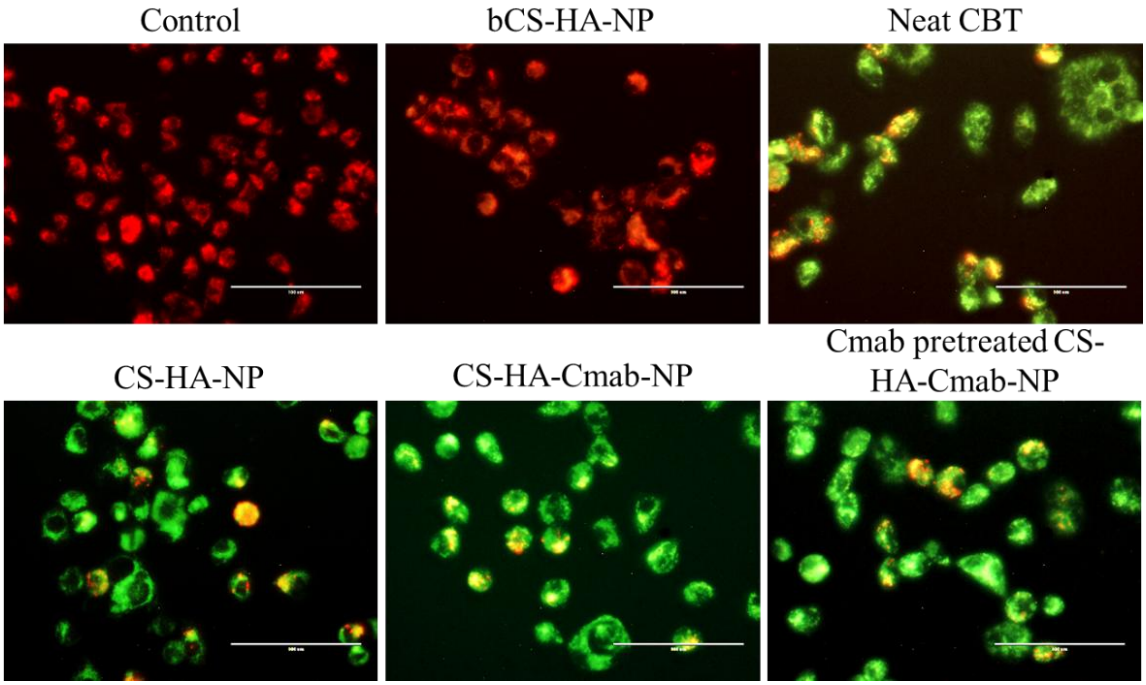

Figure 4.21 Microscopic images of JC-1-stained MDA-MB-231 cells after treatment with bCS-HA-NP, neat CBT, CS-HA-NP, and CS-HA-Cmab-NP. The control and bCS-HA-NP treated cells showed no signs of depolarization with cationic JC-1 binding to negatively charged polarized mitochondria to spontaneously form J-aggregates (red fluorescence). The CBT and CBT loaded nanoparticles show presence of JC-1 monomer (green fluorescence) due to depleted mitochondrial membrane potential **Scale bar = 100 µm**.

4.3.4.4 Assessment of mitochondrial membrane potential

The mitochondrial depolarization is one significant response of the cells treated with chemotherapeutics like taxanes. The depolarization of mitochondria is seen in cells that are in early stages of apoptosis. The extent of depolarization indicates the efficacy of the treatment in inducing a cytotoxic response. JC-1 dye is commonly used to assess mitochondrial depolarization as it gives red fluorescence after forming J-aggregates (polarized mitochondria) and green fluorescence in the case of J-monomers (formed when mitochondria are depolarized). Cabazitaxel causes depletion of mitochondrial membrane potential.

Figure 4.21 shows the microscopic images of MDA-MB-231 after exposure to various treatments for 24 h. The control and bCS-HA-NP treated cells gave red fluorescence distributed throughout the cytosol due to the formation of J-aggregates, indicating that the mitochondria remain polarized after treatment. While, the neat CBT, CS-HA-NP, and CS-HA-Cmab-NP treatments resulted in depolarization of mitochondria visually confirmed by green fluorescent signals from cells due to the presence of J-monomer. However, CS-HA-Cmab-NP treated group showed highest depolarization, followed by CS-HA-NP, suggesting enhanced intracellular accumulation of CBT due to the conjugation of Cmab on the surface of CS-HA-Cmab-NP. This was further confirmed by the blocking assay in which the cells were pretreated with Cmab resulting in reduced depolarization of cells.

4.3.4.5 Intracellular ROS levels

The mitochondrial damage observed earlier may be due to an increase in intracellular ROS after treatment with CBT-loaded nanoparticles. To compare the intracellular ROS levels DCFH-DA assay was used. DCFH-DA dye is a cell permeable dye that is converted into non-fluorescent DCFH by the esterase present in the cytosol. The DCFH is

then subsequently oxidized by the intracellular ROS to form green fluorescent 2', 7'-dichlorofluorescein (DCF). The intensity of DCF is an indicative of the intracellular ROS levels. **Figure 4.22** shows that the cells treated with CBT and CBT-loaded nanoparticles have higher ROS levels, with CS-HA-Cmab-NP treatment resulting in green fluorescence in more cells compared to CS-HA-NP and neat CBT. The results further confirm the ability of CS-HA-Cmab-NP to elicit an improved and enhanced cytotoxic response in MDA-MB-231 cells.

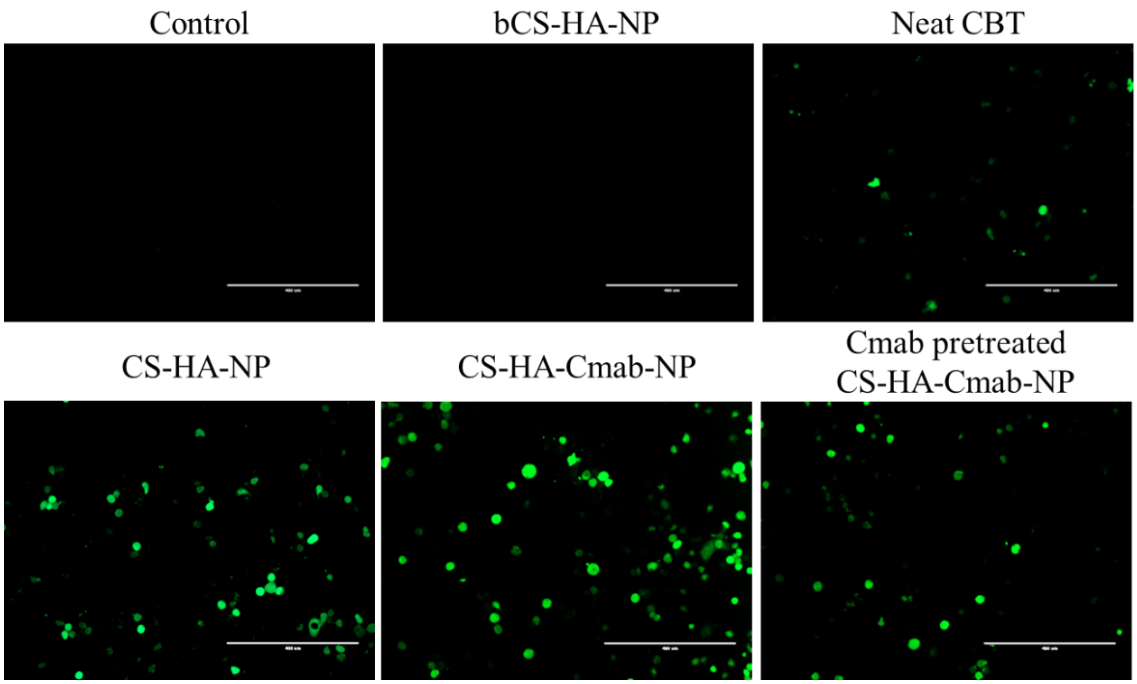

Figure 4.22 Images of MDA-MB-231 cells incubated with DCFH-DA after receiving various treatments for 24 h. The green fluorescence is due to the reduction of DCFH-DA to DCF in the presence of ROS (Scale bar = 400 µm).

4.3.4.6 Cell cycle analysis

Cell cycle analysis allows differentiation of cells in various phases of cell cycle using PI, a DNA binding dye that stoichiometrically stains the DNA. After the cells were exposed to neat CBT, bCS-HA-NP, CS-HA-NP, and CS-HA-Cmab-NP at concentration equivalent

to IC_{50} value of CS-HA-Cmab-NP for 24 h, significant increase in cell population at G2/M phase was observed (**Figure 4.23**). The cells treated with CS-HA-Cmab-NP showed 73.39% cell population in G2/M phase, while CS-HA-NP and neat CBT showed 67.95% and 32.50% cells in G2/M phase. The 2.25-fold increase in cell population in G2/M phase seen in cells receiving CS-HA-Cmab-NP in comparison to neat CBT is indicating that the augmented anti-proliferative effect is due to the enhanced intracellular accumulation of CBT. Also, a marked decline in cell population (73.39% to 66.62%) in G2/M phase was observed in the cell pretreated with Cmab before receiving CS-HA-Cmab-NP. The decline further confirmed the role of EGFR in enhancing the cellular uptake of Cmab-fuctionalized nanoparticles, consequently increasing the intracellular accumulation of CBT.

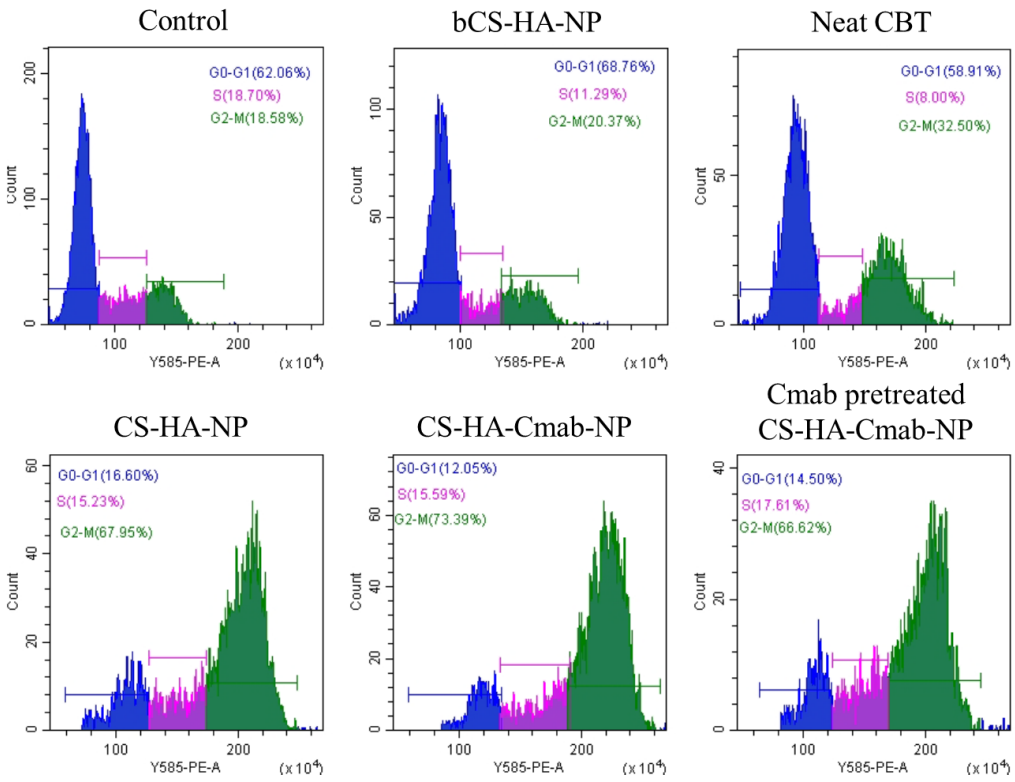

Figure 4.23 Cell cycle analysis; graphs showing population distribution of cells in different phases after incubation with various treatment for 24 h.

4.3.5 In vivo studies

4.3.5.1 Pharmacokinetic assessment

The pharmacokinetic performance of CS-HA-NP and CS-HA-Cmab-NP was compared with neat CBT after i.v. administration at a dose equivalent to 6.5 mg/kg of CBT. **Figure 4.24** shows the plasma concentration of CBT at various time points when blood samples were collected. Comparative data of parameters such as AUC^{0-t} (Area Under Curve), MRT (Mean Residence Time), t-half (half-life), etc., are mentioned in **Table 4.8**.

Table 4.8 Pharmacokinetic parameters of Neat CBT, CS-HA-NP, and CS-HA-Cmab-NP after I.V. administration (6.5 mg/kg IV, n = 12) in female Sprague Dawley rats.

Parameter	Unit	Neat CBT	CS-HA-NP	CS-HA-Cmab-NP
Lambda_z	1/h	0.04315	0.01746	0.01923
$t_{1/2}$	h	16.06107	39.68973	36.03775
T_{max}	h	0.25	0.25	0.25
C_{max}	ng/ml	13799.68	13135.24	12904.669
C_0	ng/ml	15982.744	13916.945	13523.026
C_{last_obs}/Cmax		0.02947	0.11286	0.11719
AUC 0-t	ng/ml*h	66298.649	142467.149	149312.262
AUC 0-inf_obs	ng/ml*h	75721.507	227354.055	227941.067
AUC 0-t/0-inf_obs		0.87556	0.62663	0.65505
AUMC 0-inf_obs	ng/ml*h^2	1379805.9	11216069.3	10324333.2
MRT 0-inf_obs	h	18.22211	49.33305	45.29387
V_{z_obs}	(mg/kg)/(ng/ml)	0.00199	0.00164	0.00148
Cl_{obs}	(mg/kg)/(ng/ml)/h	8.58409E-05	2.85898E-05	2.85161E-05

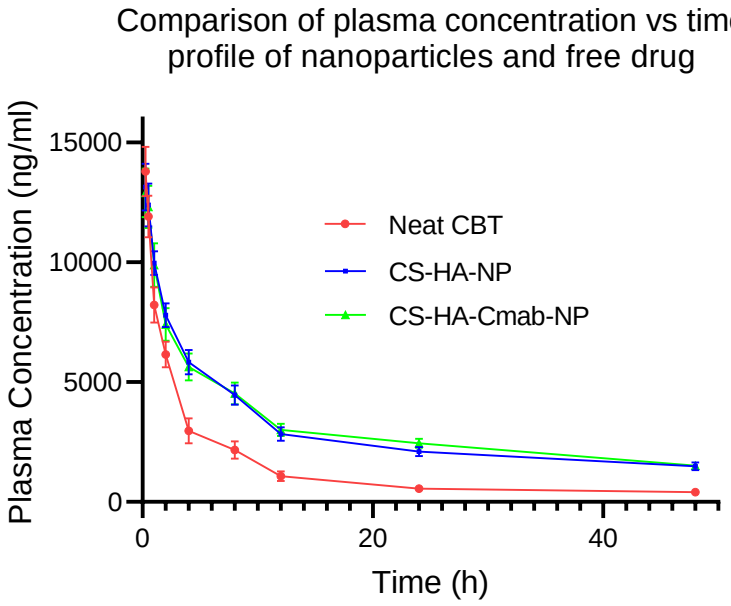

Figure 4.24 Comparative Plasma concentration vs time curve of Neat CBT, CS-HA-NP, and CS-HA-Cmab-NP. Data presented as Mean ± SD (vertical bars); n=12.

The **Figure 4.24** shows that the nanoparticles improved the plasma concentration of CBT. The half-life of nanoparticles loaded with CBT increased nearly 2.2-fold, with CS-HA-Cmab-NP exhibiting a t-half of 36.04 h compared to 16.06 h for neat CBT. The MRT of neat CBT was calculated to be 18.22 h, which increased by 2.48-fold to 45.29 h for CS-HA-Cmab-NP. A similar trend was observed for AUC^{0-t} as CS-HA-Cmab-NP showed a 2.25-fold increase compared to neat CBT. The drug loaded in the nanoparticles is released slowly at physiological pH, reducing the free drug concentration in the systemic circulation, consequently reducing metabolism and clearance. Besides, the sub-200 nm size of the particles hinders their movement across the endothelial barrier, which otherwise allows free drugs to diffuse through. Together, these characteristics of nanoparticles prevent non-selective distribution and maintain higher CBT concentrations in systemic circulation for a prolonged period compared to neat CBT, thus improving pharmacokinetic performance.

4.3.5.2 Tumor regression analysis

To determine the ability of the prepared nanoparticles to elicit anti-tumor effects, tumor regression analysis was performed in the DMBA-induced breast cancer model in female SD rats. The change in tumor volume throughout the treatment regimen was recorded, and the results are depicted in **Figure 4.25**.

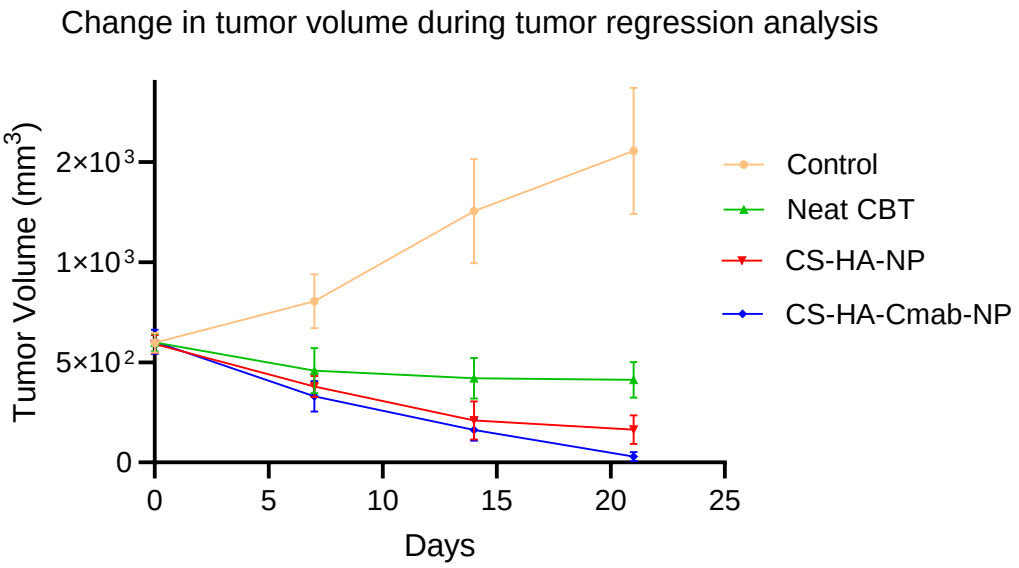

Figure 4.25 Change in tumor volume in various treatment groups during 21-day treatment period. Data presented as Mean ± SD (vertical bars); n=5

At day 7, the groups treated with neat CBT had an average 346 mm^3 lower tumor volume than the untreated group. At the same time point, the CS-HA-NP (426 mm^3) and CS-HA-Cmab-NP (475 mm^3) treated groups showed significantly (***p value <0.001) lower tumor volumes than the untreated group. At day 21, the tumor volume of neat CBT, CS-HA-NP, and CS-HA-Cmab-NP treated groups was 1143 mm^3, 1392 mm^3, and 1528 mm^3 lower than the untreated group (**Figure 4.26**).

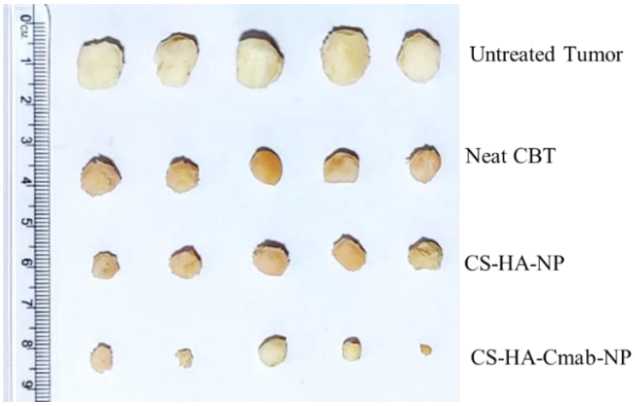

Figure 4.26 Images of tumors collected from animals after 21-day treatment. In-image cm-scale on left side.

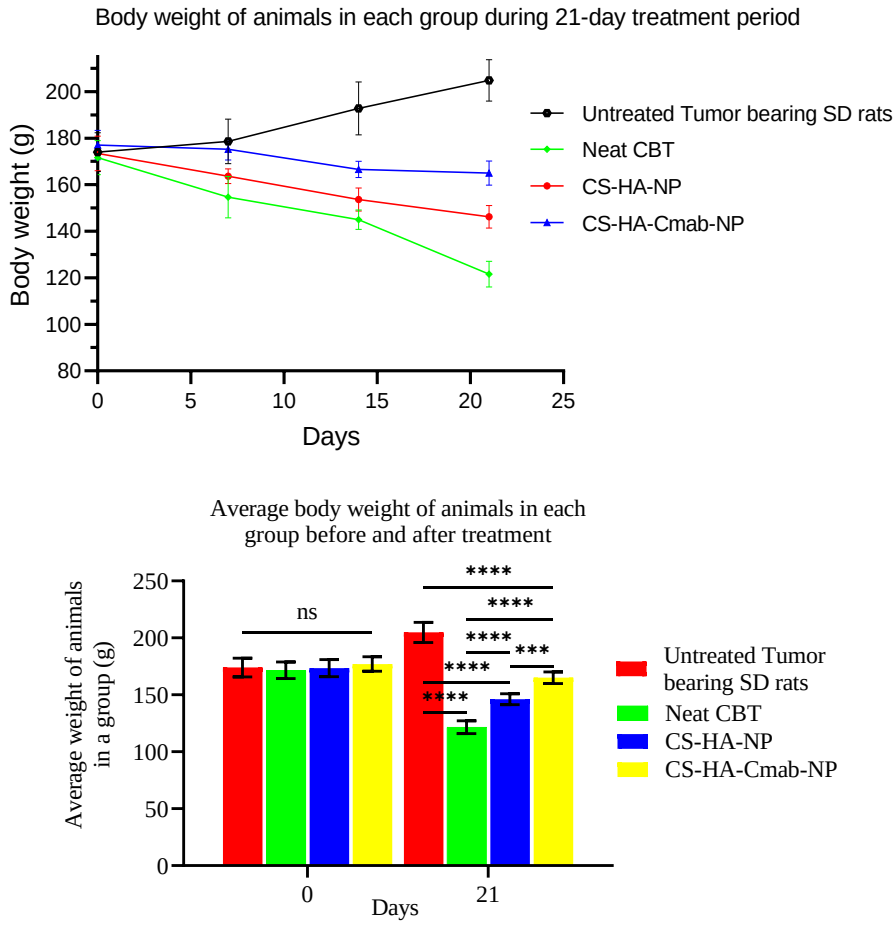

Figure 4.27 Average body weight of various treatment groups during the 21-day treatment period. Data presented as Mean ± SD; n=5. *** (p-value < 0.001), **** (p-value < 0.0001), ns (p-value > 0.05)

In other words, the nanoparticle-treated groups showed a significant reduction in tumor volume after 21 days of treatment, with the CS-HA-Cmab-NP treated group exhibiting ~21-fold and the CS-HA-NP treated group showing a 3.6-fold reduction in tumor volume. Also, the neat CBT-treated group showed a 1.4-fold reduction in tumor volume, but the tumor volume in the untreated group increased by 2.6-fold. A significant (****p-value <0.0001) change in body weight was also observed in the groups receiving treatment (**Figure 4.27**). The average reduction in body weight in neat CBT, CS-HA-NP, and CS-HA-Cmab-NP treated groups was approximately 40%, 27%, and 16%, respectively. The weight loss may largely be attributed to the systemic toxicity of CBT. The lower body weight change in CS-HA-Cmab-NP suggests the nanoparticles could effectively induce selective accumulation of CBT in target regions and reduce off-target distribution.

4.3.5.3 Survival study

The mean survival time indicates the survivability of the tumor-bearing animals during and after exposure to the respective treatment regimens. Animal deaths were noted throughout the 120-day study duration, and the Kaplan-Meier survival plot (**Figure 4.28**) was used to determine the mean survival time. The mean survival time for untreated tumor-bearing rats was calculated as 54 days and showed significant (****p-value <0.0001) improvement in the groups receiving neat CBT (76 days), CS-HA-NP (108 days), and CS-HA-Cmab-NP (>120 days). In other words, the group receiving neat CBT showed a 1.4-fold increase in mean survival time compared to the untreated group. Also, the groups exposed to CS-HA-NP and CS-HA-Cmab-NP exhibited 2-fold and >2.2-fold higher mean survival time than the untreated group. The higher probability of survival in CS-HA-NP and CS-HA-Cmab-NP treated groups indicates their improved safety and higher efficacy compared to neat CBT treatment.

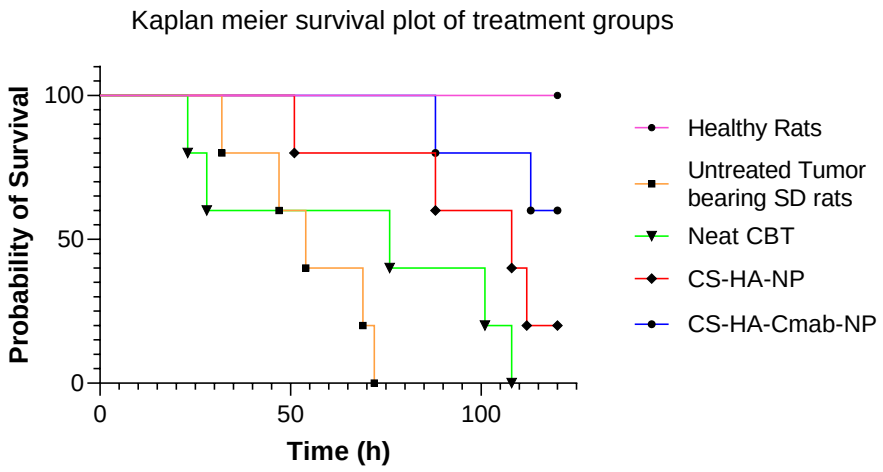

Figure 4.28 Kaplan Meier survival plot of various treatment groups (up to 120 days).

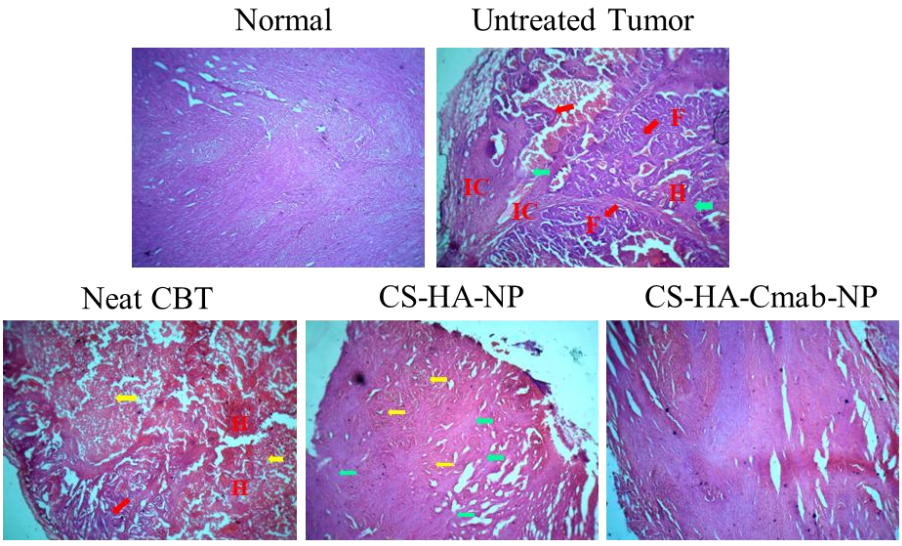

Figure 4.29 H&E-stained histological images of normal and tumor tissue after 21-day treatment period (images shown are captured with 4X lens).

4.3.5.4 Histological assessment of tumors and organs

H&E staining was utilized to detect histological changes after tumor induction and therapy with various formulations (**Figure 4.29**). The normal group had normocellular tissue structure with no evidence of proliferating cells [143–145].

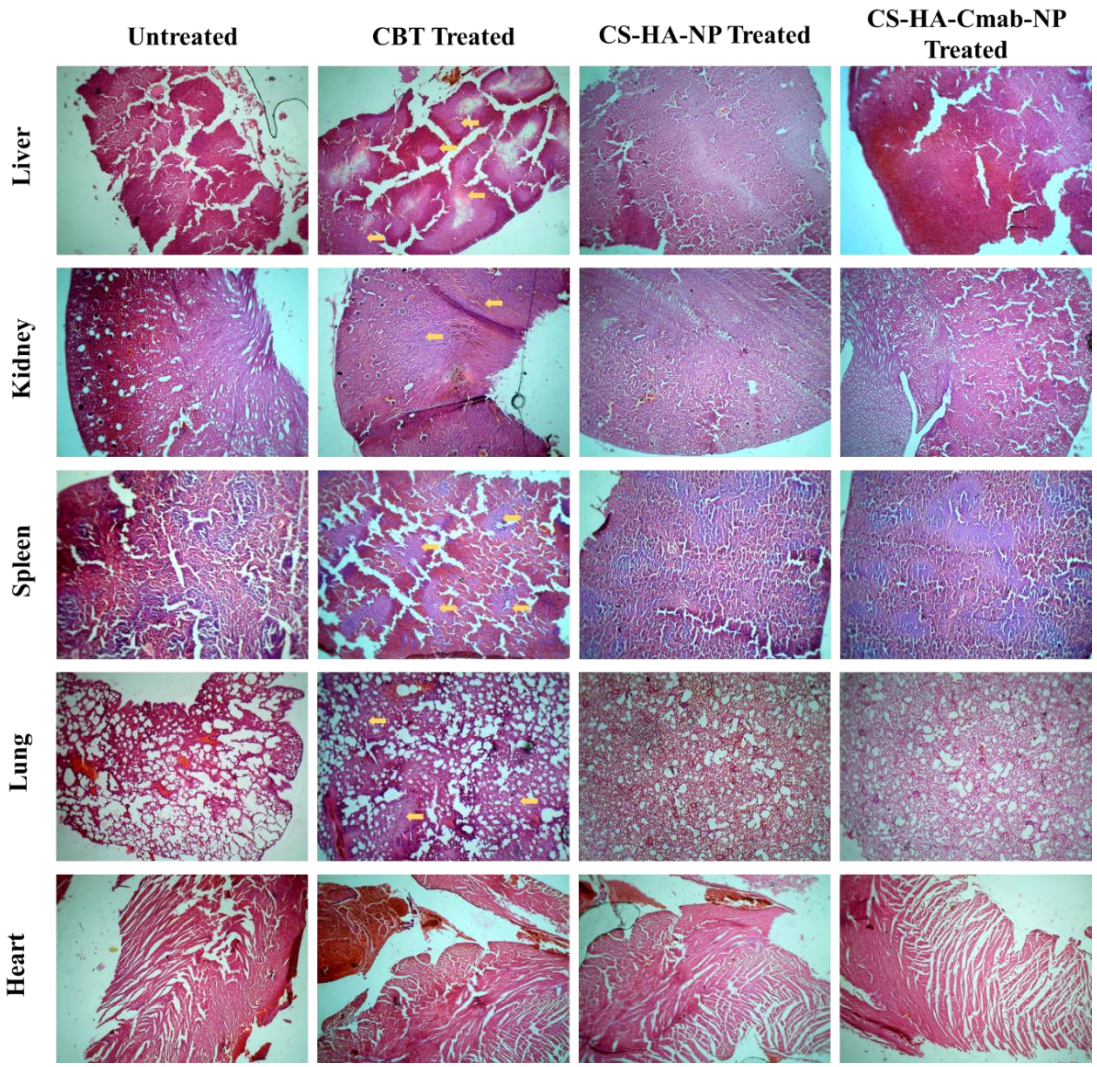

Figure 4.30 H&E-stained histological images of organs collected from various treatment groups after 21-day treatment period (images shown are captured with 4X lens).

The untreated tumor-bearing SD rats group demonstrated evidence of highly proliferating tissues, indicating breast cancer cells (red arrows). The carcinoma exhibited enhanced proliferation and growth of terminal lobular units, as well as signs of invasive carcinoma (IV) expanding into the surrounding fat tissue/adipocytes [146]. The cancer had glandular atrophy with surrounding stromal fibrosis (fibroadenoma, F) and breast hyperplasia (H) [144]. CBT treatment controlled the fibroadenoma, although there were still visible signs of breast hyperplasia area and cancer cell proliferated tissue. CS-HA-NP was found to be beneficial in treating breast cancer even with minimal signs of cancer cells remain

(yellow arrow) and mucin (green arrow) [145]. While, the CS-HA-Cma-NP treated groups demonstrated almost complete cancer elimination with a reconstituted thick mass, similar to normocellular tissue structure [143]. To investigate the safety of nanoformulations over neat CBT, all major organs including liver, kidney, spleen, lung, and heart of each group were examined for histological changes. CBT treated groups showed few histological changes (yellow arrow) as signs of organ toxicity **Figure 4.30**. In contrast, CS-HA-NP and CS-HA-Cmab-NP had tissue structure of all organs similar to untreated groups, and thus not exhibited much side effects. This could be due to the preferential accumulation of a major portion of nanoparticles to the target site, avoiding off-target drug distribution and thus minimizing organ toxicity.

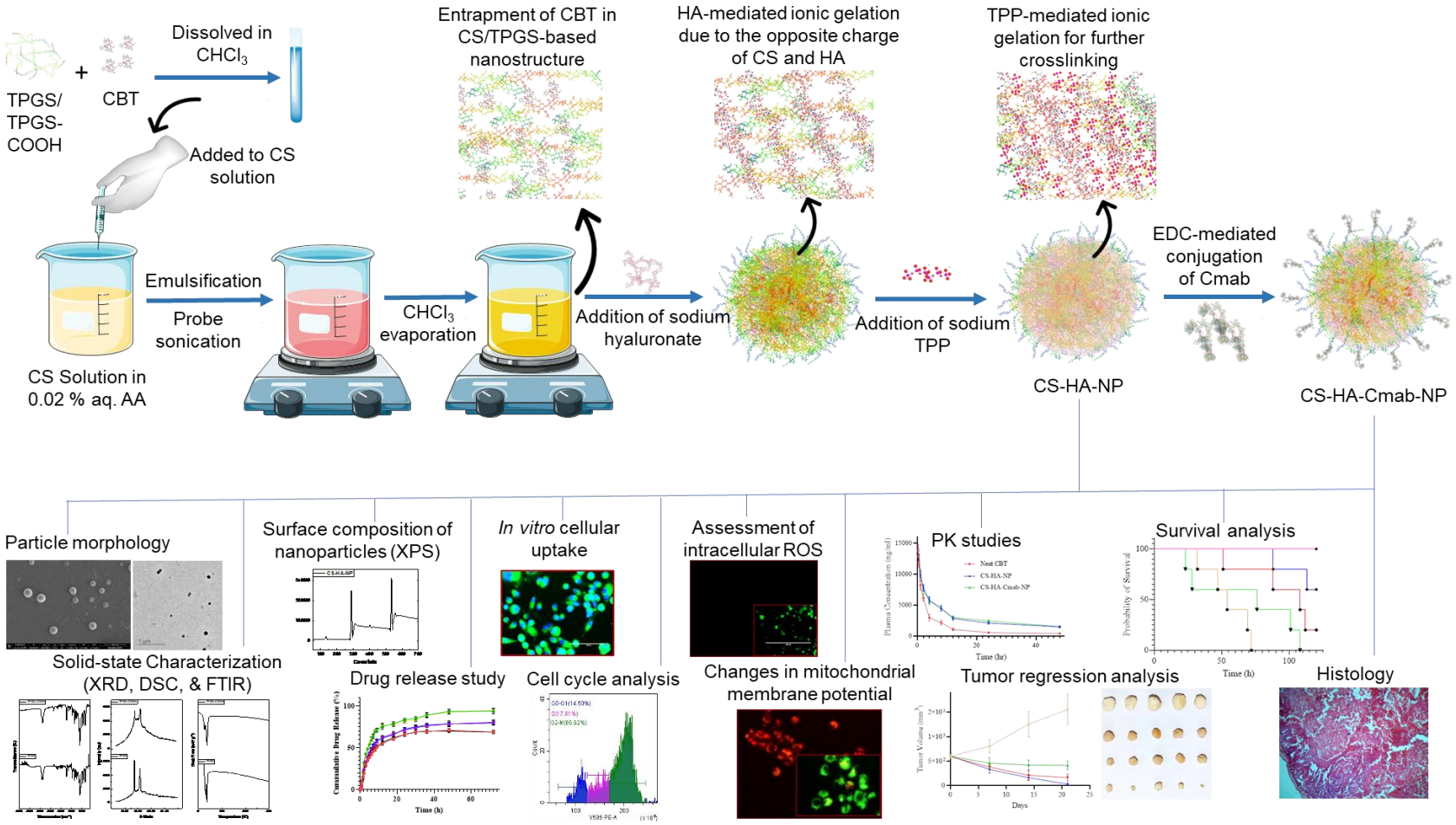

Figure 4.31 Graphical Summary of Objective 1